HHS Public Access

Author manuscript

Nature. Author manuscript; available in PMC 2020 December 24.

Published in final edited form as:

Nature. 2020 August ; 584(7820): 310–314. doi:10.1038/s41586-020-2469-4.

Structures of metabotropic $GABA_B$ receptor

Makaía M. Papasergi-Scott[1,2,4], **Michael J. Robertson**[1,2,4], **Alpay B. Seven**[1,2], **Ouliana Panova**[1,2], **Jesper M. Mathiesen**[3], **Georgios Skiniotis**[1,2,*]

[1]Department of Molecular and Cellular Physiology, Stanford University School of Medicine, Stanford, CA 94305, USA.

[2]Department of Structural Biology, Stanford University School of Medicine, Stanford, CA 94305, USA.

[3]Department of Drug Design and Pharmacology, Faculty of Health and Medical Sciences, University of Copenhagen, Copenhagen, Denmark.

[4]These authors contributed equally to this work.

Abstract

GABA (γ-aminobutyric acid) stimulation of the metabotropic $GABA_B$ receptor results in prolonged inhibition of neurotransmission that is central to brain physiology[1]. $GABA_B$ belongs to the Family C of G protein-coupled receptors (GPCRs), which operate as dimers to relay synaptic neurotransmitter signals into a cellular response through the binding and activation of heterotrimeric G proteins[2,3]. $GABA_B$, however, is unique in its function as an obligate heterodimer in which agonist binding and G protein activation take place on distinct subunits[4,5]. Here we show structures of heterodimeric and homodimeric full-length $GABA_B$ receptors. Complemented by cellular signaling assays and atomistic simulations, the structures reveal an essential role for the $GABA_B$ extracellular loop 2 (ECL2) in relaying structural transitions by ordering the linker connecting the extracellular ligand-binding domain to the transmembrane region. Furthermore, the ECL2 of both $GABA_B$ subunits caps and interacts with the hydrophilic head of a phospholipid occupying the extracellular half of the transmembrane domain, thereby providing a potentially crucial link between ligand binding and the receptor core that engages G protein. These results

*To whom correspondence should be addressed: yiorgo@stanford.edu.

Author contributions

M.M.P-S. designed and cloned $GABA_B$ constructs, expressed and purified all proteins, collected and processed cryoEM data. M.J.R. built and refined the structure from cryoEM density maps and set up, performed, and analyzed molecular simulations. A.B.S. and O.P. assisted with cryoEM data collection and processing. J.M.M. performed and analyzed cellular signaling experiments. M.M.P-S., M.J.R, J.M.M., and G.S. interpreted results. M.M.P-S., M.J.R., J.M.M., and G.S. wrote the manuscript with O.P. and A.B.S. providing input. G.S. supervised the project.

Competing interests

The authors declare no competing interests.

Data Availability

All data generated or analyzed during this study are included in this published article and the Supplementary Information. CryoEM maps of $GABA_B$ heterodimer and $GABA_{B1b}$ homodimer have been deposited in the Electron Microscopy Data Bank under accession codes EMD-21533 and EMD-21534, respectively. The atomic coordinates of $GABA_B$ heterodimer and $GABA_{B1b}$ homodimer have been deposited in the Protein Data Bank under the accession codes 6W2X and 6W2Y, respectively.

provide a starting framework to decipher mechanistic modes of signal transduction mediated by $GABA_B$ dimers and have important implications for rational drug design targeting these receptors.

The neurotransmitter GABA is primarily responsible for synaptic inhibition throughout the nervous system via activation of $GABA_A$ ion channels and pre- and postsynaptic $GABA_B$ receptors. $GABA_B$ stimulation of the $G_{i/o}$ class of heterotrimeric G proteins results in a prolonged decrease in neuronal excitability via the inhibition of adenylyl cyclase and voltage-gated Ca^{2+} channels, as well as the opening of G protein-coupled inward rectifying potassium channels[2,3,6]. Abnormal execution of $GABA_B$ signaling causes multiple neuropsychiatric diseases and the receptor is an attractive drug target for a range of disorders including drug addiction, pain, epilepsy, spasticity, anxiety, and gastroesophageal reflux disease[7,8].

Family C GPCRs represent ~20 receptors including $GABA_B$, metabotropic glutamate receptors (mGlu1–8), the calcium sensing receptor, as well as two taste and several orphan receptors[9,10]. These receptors operate as obligate dimers, with each subunit composed of a bi-lobed extracellular ligand-binding domain termed the Venus flytrap (VFT) and a 7-transmembrane domain (7TM) connected via a linker region[11]. Crystallographic studies of VFTs from various Family C members, including $GABA_B$, show that agonist binding rearranges the VFTs in a way that would bring the linker regions into close proximity[12,13]. All Family C GPCRs contain a cysteine-rich domain (CRD) within the linker region, except for $GABA_B$ which has a relatively short linker. Our recent mGlu5 structures showed that the CRD interacts with ECL2 of the transmembrane region, thereby transducing conformational changes 120Å from the ligand-binding site on the VFT to the 7TM domain where G protein activation occurs[14]. Given that $GABA_B$ lacks a CRD, the structural communication between an agonist-bound VFT and the 7TM domains remains unclear.

Furthermore, unlike other Family C GPCRs, $GABA_B$ is an obligate heterodimer of dissimilar subunits, $GABA_{B1}$ and $GABA_{B2}$[15]. Agonist binding occurs only on the VFT of $GABA_{B1}$, while G protein coupling and activation occurs exclusively through $GABA_{B2}$[4,5]. Therefore, besides its pharmacological interest, $GABA_B$ presents an ideal model system to study trans-activation mechanisms of dimeric Family C GPCRs. Such studies, however, have been limited by the lack of structural information on full-length $GABA_B$, restricting our ability to understand how agonist binding to $GABA_{B1}$ results in G protein activation on the intracellular side of $GABA_{B2}$. In the present study we employed single-particle cryo-electron microscopy (cryoEM), atomistic simulations, and cellular signaling assays to obtain structural and mechanistic insights into full-length $GABA_B$ receptor complexes.

For structural studies, we co-expressed recombinant constructs of human $GABA_{B1b}$ and $GABA_{B2}$ in insect cells and purified the $GABA_B$ heterodimer by tandem affinity-chromatography in the presence of the inverse agonist CGP55845[16]. The structure of the inactive detergent solubilized $GABA_B$ heterodimer was determined at a global indicated resolution of 3.6 Å (Fig. 1, Extended Data Figs. 1, 2a, and Table 1). The cryoEM map resolved the entire $GABA_B$ apart from the C-terminal coil-coil domain that appears to be flexible in relation to the transmembrane regions. Additionally, a focused map of the extracellular region at a resolution of 3.5 Å provided improved density for the linker regions

and assisted with modeling (Extended Data Fig. 1). The asymmetric protomers, $GABA_{B1}$ and $GABA_{B2}$, share a similar secondary structure and arrangement but are distinguished by differential glycosylation and a well-resolved ligand density within the $GABA_{B1}$ VFT domain that is absent in $GABA_{B2}$ (Fig. 1, Extended Data Figs. 3 and 4a). The upper VFT lobes of $GABA_B$ form a junction, while the lower VFT lobes are separated by ~20 Å (Fig. 1, Extended Data Fig. 3). The ligand, CGP55845, adopts a horseshoe-like conformation that was confirmed by GemSpot[17], closely resembling the crystal structure of the $GABA_{B1}$ VFT domain in complex with the inhibitor CGP54626 (Extended Data Fig 3)[12,16]. We also observe a small spherical density in $GABA_{B1}$ that appears to be interacting with the backbone carbonyl of G277 in addition to several anionic groups and a tyrosine, raising the possibility of a divalent cation in that location (Extended Data Fig. 3e).

Inactive $GABA_B$ assumes a similar overall morphology to the apo-state structure of mGlu5[14], while the most substantial differences arise within the linker region (Fig. 1b). Bridging the VFT and 7TM domains, an ~20 residue linker forms a β-sheet in conjunction with the ECL2. Notably, the length of the $GABA_B$ receptor ECL2 is nearly twice that of mGlu5 (Fig.1, Extended Data Fig. 4b). In the absence of CRDs, the β-sheet structure of the $GABA_B$ linker in complex with ECL2 orders this region with the additional ECL2 length thus allowing 7TM and VFT domain coupling for signal transduction. Molecular dynamics (MD) simulations support the structural stabilization of the linker through the β-sheet formation. After 200 ns in all simulations the linker and ECL2 continued to adopt a stable structure even in the absence of VFT domains, although a slight downward rotation in β-sheet orientation was observed (Extended Data Fig. 5). To further examine the involvement of the ECL2 in receptor activation, we employed a functional assay with a chimeric $G\alpha_{o/q}$, whereby the $G_{i/o}$-coupled $GABA_B$ receptor can couple to the PLC pathway[3,18]. Accumulation of the downstream metabolite IP_1 by LiCl was measured by an established assay[19], thereby monitoring GABA-stimulated and basal receptor activity (Fig. 1c). ECL2 shortening was generally inhibitory to the proper membrane trafficking of the $GABA_B$ subunits. Accordingly, we normalized the transfected DNA to obtain similar expression levels between constructs (Extended Data Fig. 6a). The partial deletion of the $GABA_{B1}$ ECL2 loop (Δ627–634), comprising the unstructured tip of the loop nearest the VFT, produced an increase in basal activity but did not affect GABA E_{max} when expressed with wild-type $GABA_{B2}$ (Fig. 1d). These findings indicate that abrogating the ECL2-linker allows flexibility in the $GABA_{B1}$ VFT relative to the rest of the receptor dimer, resulting in activation through the $GABA_{B2}$ VFT/7TM route in the absence of agonist[20]. In contrast, the partial deletion of the $GABA_{B2}$ ECL2 (Δ631–638) did not affect basal activity but produced an increase in GABA E_{max} and a decrease in GABA potency when compared to wild-type receptor expressed to similar levels at the cell surface, indicating that the $GABA_{B2}$ ECL2 may be partially inhibitory (Fig. 1d, Extended Data Fig. 6a). When both receptors contain a truncated ECL2, we observed a decrease in GABA E_{max}, suggesting that at least one VFT domain must be structurally coupled through the extended ECL2/linker for full activation (Fig. 1d). Collectively, these data support a bimodal transactivation mechanism of $GABA_B$ in which agonist binding on the $GABA_{B1}$ receptor can proceed from the $GABA_{B1}$ VFT down to the $GABA_{B1}$ 7TM region to enact changes in $GABA_{B2}$ that promote G protein activation, and also activate the $GABA_{B2}$ 7TM directly through the $GABA_{B2}$ VFT domain.

Besides the VFTs and the C-terminal coiled-coil, we observe that inactive $GABA_B$ forms an additional dimer interface between TM3 and TM5 from each monomer of the heterodimer (Fig. 1, Fig. 2). The interface is formed by ionic interactions between residues on the intracellular side of each receptor, $H572^{(TM3)}$ and $E673^{(TM5)}$ on $GABA_{B1}$ and $H579^{(TM3)}$ and $E677^{(TM5)}$ of $GABA_{B2,}$ with further stabilization through aromatic residues along the same helices (Fig. 2b, c). Observed elongated densities, likely corresponding to glyco-diosgenin (GDN) and/or cholesteryl hemisuccinate used in purification, packed between the extracellular sides of the two 7TM regions may also stabilize the interface (Fig. 1a). The dimer interface is in contrast to the inactive mGlu5 receptor where ~16Å separates the 7TM domains (Fig. 2a)[14]. To probe the significance of these interactions, we mutated the TM3/TM5 interface, and performed IP_1 accumulation assays (Fig. 2d, e, Extended Data Fig. 6). Notably, mutation of either H579 or E677 on $GABA_{B2}$ or mutation of both E673 and H572 on $GABA_{B1}$ increased the basal activity of the receptor, suggesting that the TM3/TM5 interface is inhibitory to signaling in the absence of agonist, which further supports the transactivation mechanism described above (Fig.2, Extended Data Figs. 6b–e). When expressed at the cell surface alone, the H579/E677 double mutant of $GABA_{B2}$ exhibited a slight increase in basal activity compared to $GABA_{B2}$ alone (Extended Data Fig. 6d). These findings further support a role of an intra-protomer H579/E677 interaction in $GABA_{B2}$ to assist stabilizing an auto-inhibited state, and are consistent with the lack of constitutive activity by the $GABA_{B2}$ ECL2 (Δ631–638) deletion mutant.

The most unexpected observation in the transmembrane region of both monomers of $GABA_B$ is a wishbone-shaped density occupying the extracellular half of each 7TM core. The bifurcated density, which is better resolved within the $GABA_{B1}$ helical bundle, corresponds to a phospholipid (Fig. 3, Extended Data Fig. 2). Considerations of the size and shape of the density, surrounding amino acid environment within the 7TM core, and known phospholipid composition in Sf9 insect cells, led us to infer that the density in $GABA_{B1}$ and likely $GABA_{B2}$ corresponds to phosphatidylethanolamine (PE) (Fig. 3, Extended Data Fig. 7). However, it is possible that the observed density is the result of a heterogeneous mixture of phospholipids. The observation of the phospholipid is particularly intriguing, as no other GPCR structure has revealed a two-chained phospholipid within this space. Although a lipid-activated subfamily within Family A GPCRs exists, known ligands are single-acyl-chain lipids, eicosanoids, and sterols[21]. Notably, $GABA_B$ residues in the extracellular loops, including ECL2, and TM3 of $GABA_B$ coordinate the polar headgroup of the phospholipid, resulting in a ‘lid’ over the 7TM cavity that resembles the lipid-binding Family A GPCRs. The remaining hydrophilic atoms in the lipid appear solvent-exposed, whereas the lipid tails are buried deep into the hydrophobic portion of the transmembrane cavity (Fig. 3b, c). The presence of the 7TM lipid in our cryoEM structures suggests it is bound tightly, as also suggested by its retention during detergent solubilization of the receptor. Additionally, a conserved TM6 tryptophan, which acts as an activating “toggle-switch” in other Family C GPCRs[22,23], is replaced by cysteine in both $GABA_{B1}$ and $GABA_{B2}$ (Extended Data Figs. 4c, d). This replacement is essential, as any probable tryptophan rotamer at that position would clash sterically with the bound phospholipid.

The presence of lipid in the 7TM core suggests it may have a physiological role in the structural and functional integrity of the transmembrane bundles, occupying a region that

corresponds to the ligand-binding site in other GPCR classes (Extended Data Fig. 4). Moreover, given the role of the ECL2 in coupling the VFT domains to the 7TM regions, it is conceivable that interactions of the phospholipid with the ECL2 are essential in increasing the stability of the linker region and also participate in relaying structural transitions from the VFTs to the 7TM core. Markedly, mutations designed to displace lipid tails in the 7TM core, $GABA_{B1}$ L553W and $GABA_{B2}$ L560W, decrease basal activity and potency of GABA while increasing GABA E_{max}, whereas mutation of the arginine coordinating the headgroup of the phospholipids, $GABA_{B1}$ R549A and $GABA_{B2}$ R556A, results in increases in both $GABA_B$ basal activity and receptor response to GABA (Fig. 3d, Extended Data Figs. 6f and g). Collectively, these results indicate that destabilization of phospholipid in the core affects receptor activation, and it is thus conceivable that the lipid directly modulates receptor activity as a result of ECL2 movements in native $GABA_B$. To further probe the role of phospholipid we employed a range of atomistic simulations with the $GABA_B$ receptor system. We initiated simulations of the $GABA_B$ 7TM and linker with the VFTs removed, both with and without lipid. The simulations revealed that without lipid the transmembrane helices begin to collapse into the core with mean decreases in cavity volume of ~30% (Fig. 3, Extended Data Fig. 5, Supplementary Data 1 and 2), suggesting a strongly coupled interplay between the phospholipid and 7TM core. Alternatively, multiple simulations that started without lipid in the TMs showed lipid tails from the bilayer entering the receptor hydrophobic cavity below residue Y661, at a site akin to where the tail protrudes in our cryoEM structure. Remarkably, peripheral lipid tail insertion in simulations correlated with circumvention of the 7TM cavity collapse (Extended Data Fig. 5). In one simulation, after 200 ns we observed a lipid that had inserted both of its hydrocarbon tails into the receptor core. Extending the simulation by an additional 100 ns revealed the headgroup has moved over the top of the receptor, indicating lipid entry may occur as a stepwise process, with lipid tail entry sliding between TM5 and TM6 and followed by the entire lipid (Extended Data Fig. 5). Although it is probable that lipid insertion into the 7TM core occurs concurrently with helix insertion into the membrane during protein folding, these results suggest a clear tendency for phospholipids to insert at that position in a mature receptor.

Pharmaceuticals targeting the $GABA_B$ receptor and other Family C GPCRs are proposed to function either at the orthosteric ligand binding site or allosterically within the transmembrane core, like Family A orthosteric ligands. However, the bound-phospholipid would appear to occlude the binding of allosteric modulators analogous to those used to target other Family C receptors[24]. Consequently, potential $GABA_B$ allosteric modulators would need to either displace the core lipid or bind at an alternative site peripheral to the bundle.

While pure $GABA_B$ heterodimer was obtained by tandem affinity purification of receptor constructs with distinct tags, when both subunits contain an N-terminal FLAG tag we also purified a significant fraction (> 40%) of $GABA_{B1}$ homodimers. In cells, an ER retention signal within the $GABA_{B1}$ coil-coil domain prevents $GABA_{B1}$ from reaching the plasma membrane unless masked by the $GABA_{B2}$ C-terminus or other interacting partners[25,26]. Thus, the presence of $GABA_{B1}$ homodimer in our preparation is likely due to the persistence of internal membranes during the purification procedure. However, multiple studies have suggested a physiologic role for $GABA_{B1}$ homodimers within some cell types of the nervous

system and gastrointestinal tract that express $GABA_{B1}$ isoforms in the absence of $GABA_{B2}$[27–32]. Although it is yet unclear how homodimeric $GABA_{B1}$ functions in the absence of $GABA_{B2}$ G protein coupling, we sought to obtain further mechanistic insights into the $GABA_B$ system and obtained the structure of the $GABA_{B1b}$ homodimer at a global indicated resolution of 3.2 Å (Fig. 4, Extended Data Figs. 2, 8, and Table 1).

The structure of the $GABA_{B1}$ homodimer shows that both VFTs are liganded and the monomers assume a roughly 2-fold symmetric arrangement. The individual lobes of each VFT domain are in an open-conformation and superimposable with the $GABA_{B1}$ subunit VFT in the inactive heterodimer (Fig. 4b). Remarkably, despite the individual protomer conformation, the VFT homodimer adopts the same overall conformation as the crystal structure of agonist-bound $GABA_B$ VFTs (PDB:4MS4)[12] due to an almost identical upper lobe interaction interface (Fig. 4b). Correspondingly, the lower lobes of the receptor are brought into proximity and the receptor adopts a more compact state shortening the distance between the VFTs and the 7TMs (Fig. 4). Compared to the heterodimer, the 7TM domains in the $GABA_{B1}$ homodimer are rotated to form a TM6-TM6 interface (Fig. 4c). This is in agreement with cross-linking experiments that identified a TM6-TM6 interaction upon agonist-induced stimulation of the heterodimer[33], and agrees with structural rearrangements of mGlu5 upon agonist stimulation (Fig. 4d)[14]. Furthermore, the relative arrangement of the VFT and transmembrane regions are strikingly similar to the activated state of near full-length mGlu5[14] (Extended Data Fig. 8). Thus, the conformation observed in the $GABA_{B1}$ homodimer may provide valuable hints into the architecture of the active state $GABA_B$ receptor (Fig. 4). Along the same lines, $GABA_B$ chimera studies show that replacement of one of the 7TM domains of the $GABA_{B1}$ homodimer with that of the $GABA_{B2}$ receptor, thus enabling G protein coupling, produces a constitutively active receptor that is not additionally stimulated by GABA[34,35]. Hence, the relative positioning of the VFT domains, as observed in the $GABA_{B1}$ homodimer structure, appears to be sufficient to stabilize an active conformation, presumably through the linkage of VFT to 7TM domains to reorient the helical interface. Since $GABA_{B1}$ in the homodimer is bound to an inverse agonist, the adoption of an ‘active-like’ global conformation of the VFT domains must be irrespective of the ligand, likely due to differences in the interaction interface of the VFT N-terminal lobes in comparison to the same interface in the heterodimer.

Collectively, our structures, cellular signaling assays, and atomistic simulations provide crucial insights into mechanistic aspects of $GABA_B$ signaling. The extended ECL2 and its interaction with the linker region appears to compensate for the lack of CRD in $GABA_B$ compared to all other Family C receptors, and thus also transduce conformational changes from the VFT to the 7TM domains. The phospholipid occupying the 7TM core is important for the integrity of the transmembrane domains in both $GABA_B$ subunits, while also structurally coordinating the critical ECL2 region. Our findings support a model in which agonist binding to $GABA_{B1}$ results in VFT dimer compaction that reorients the protomers via the linker/ECL2. Such conformational change would drive the 7TM domains to twist away from an auto-inhibited state mediated by the inactive TM3/TM5 interface, thereby forming a new TM6 helical interface. Although currently unclear, the activating transitions within the $GABA_{B2}$ 7TM are likely mediated both through the newly formed TM6/TM6 interface and propagation through its own ECL2, as supported by our functional assays. An

intriguing possibility is that the phospholipid may act as a sensor of changes in VFT and ECL2 conformations that would result in activating transitions within the 7TM domain of $GABA_{B2}$ to prime it for G protein engagement. Addressing these questions will require detailed structural studies of active state heterodimer alone and in complex with G protein engaging the receptor core. The present work, along with our recent studies on mGlu5, form a starting structural framework to decipher the enigmatic signal transduction mechanism of $GABA_B$ and Family C GPCRs in the context of full-length receptors.

Materials & Methods

Cloning

The cDNA clone for human $GABA_{B2}$ receptor (Accession: NM_005458) in pcDNA3.1$^+$ was obtained from the cDNA Resource Center (www.cdna.org); and the cDNA clone for human $GABA_{B1b}$ was purchased from Horizon Discovery (Accession: BC050532, Clone ID: 5732186). Primers were designed to include a hemagglutinin (HA) signal sequence[36] in the place of authentic signal sequences of each receptor, thus removing the first 29 residues of $GABA_{B1}$ and 41 residues of $GABA_{B2}$. Both the authentic signal sequence and the HA sequence are cleaved during processing; therefore, the substitution does not result in a change of sequence in the mature receptor. For purification of receptors for cryoEM studies, $GABA_B$ constructs were subcloned into the pFastBacDual vector (Invitrogen) with N-terminal Flag epitope (DYKDDDD) following the HA signal sequence and/or C-terminal hexa-histidine (His6) tags, so that the following constructs were produced: HA-FLAG-$GABA_{B1}$(30–844)-His6, HA-$GABA_{B1}$(30–844)-His6, and HA-FLAG-$GABA_{B2}$(41–941). For signaling assays the HA-FLAG-$GABA_{B1}$(30–844)-His6 and a HA-HA-$GABA_{B2}$(41–941)-construct (where FLAG tag was replaced by the HA epitope tag YPYDVPDYA) were subcloned into pcDNA3.1(+). The primers (Integrated DNA Technologies) used to sub-clone $GABA_B$ included: EcoRI-HA-Flag-$GABA_{B1,}$5’-GCGCGCGAATTCATGAAGACGATCAT

CGCCCTGAGCTACATCTTCTGCCTGGTGTTCGCCGATTACAAGGACGACGATGAC AAGTCCACTCCCCCCATCTCCCG-3’ ; $GABA_{B1}$-His6-SalI, 5’-GCGCGCGTCGACTTAATGATGATGATG

ATGGTGCTTATAAAGCAAATGCAC-3’; $GABA_{B1}$-SalI 5’-GCGCGCGTCGACTTACTTATAAAG

CAAATGCAC-3’; EcoRI-HA-FLAG-$GABA_{B2}$, 5’-GCGCGCGAATTCATGAAGACGATCATCGCC

CTGAGCTACATCTTCTGCCTGGTGTTCGCCGATTACAAGGACGACGATGACAAGT GGGCGCGGGGCGCCCCC-3’; $GABA_{B2}$-His6-SalI, 5’-GCGCGCGTCGACTTAATGATGATGATGATGGTG

CAGGCCCGAGACCATGAC-3’; $GABA_{B2}$-SalI, 5’-GCGCGCGTCGACTTACAGGCCCGAGACCA

TGAC-3’. To generate $GABA_B$ mutants PCR reactions were conducted with either PfuTurbo or Q5 polymerase using the following pairs of primers and pcDNA3.1$^+$neo containing either

HA-FLAG-$GABA_{B1b}$ or HA-HA-$GABA_{B2}$: $GABA_{B1b}$ H572A, 5'-GGTGGGTCGCCACGGTCTTC-3' and 5'-GAAGACCGTGGCGACCCACC-3'; $GABA_{B1b}$ E673A, 5'- CTTGCTTATGCTACCAAGAG-3' and 5'-CTCTTGGTAGCATAAGCAAG-3'; $GABA_{B2}$ H579A, 5'-CTGGAGAGTCGCTGCCATCTTCAA-3' and 5'-TTGAAGATGGCAGCGACTCTCCAG-3'; $GABA_{B2}$ E677A, 5'-CTTAGCTTGGGCTACCCGCAAC-3' and 5'- GTTGCGGGTAGCCCAAGCTAAG-3'; $GABA_{B1}$ (Δ627–634), 5'- CTTGGCAAATGTCTCAATGGTC-3' and 5'-GTCTCTATTCTGCCCCAGC-3'; $GABA_{B2}$ (Δ631–638), 5'-ATCTCCATCCGCCCTCTCC-3' and 5'-CATGCTGTACTTCTCCACTG-3'; $GABA_{B1}$ R549A, 5'- CTGCCAGGCCGCCCTCTGGCTCCTG-3' and 5'-ACGAAAGGGAACTGG-3'; $GABA_{B2}$ R556A, 5'-GCACCGTCGCTACCTGGATTCTC-3' and 5'- AAA GTG TTT CAA AGG-3'; $GABA_{B1}$ L553W, 5'- CTCTGGCTCTGGGGCCTGGGCTTTAG-3' and 5'-GCGGGCCTGGCAGACG-3'; $GABA_{B2}$ L560W, 5'-GGACCTGGATTTGGACCGTGGGCTAC-3' and 5'-TGACGGTGCAAAGTG-3'.

Expression and Purification

Spodoptera frugiperda (Sf9) insect cells (Expression Systems) were co-infected at a density of ~2.0×10^6 cells/mL with HA-FLAG-$GABA_{B2}$ baculovirus and either HA-FLAG-$GABA_{B1b}$-His6 or HA-$GABA_{B1b}$-His6 baculovirus at a multiplicity of infection (M.O.I.) between 3.0 – 5.0. During expression, cells were treated with 5 μM CGP55845 (Hello Bio, Inc.). At 48 hours post-infection cells were harvested by centrifugation, washed once with phosphate-buffered saline containing protease inhibitors (leupeptin, soybean trypsin inhibitor, N-*p*-Tosyl-L-phenylalanine chloromethyl ketone, Tosyl-L-lysyl-chloromethane hydrochloride, phenylmethylsulfonyl fluoride, aprotinin, bestatin, pepstatin) and 5 μM CGP55845. Cell lysis was achieved through nitrogen cavitation in buffer containing 20 mM HEPES, pH 7.5, 150 mM NaCl, 1 mM EDTA, 10 μM CGP55845, 2 mM $MgCl_2$, nuclease, and protease inhibitors. The whole-cell lysate was centrifuged at 1,000 xg to remove nuclei and unbroken cells. The supernatant was centrifuged at 100,000 xg to isolate the membrane fraction. Membranes were resuspended by Dounce homogenization in buffer containing 20 mM HEPES, pH 7.5, 150 mM NaCl, 2 mM $MgCl_2$, 1 mM EDTA, 2 mg/mL iodoacetamide, 10 μM CGP55845, 1% n-Dodecyl β-D-maltoside (DDM), 0.2% Sodium cholate, 0.2% Cholesterol hemisuccinate (CHS), nuclease, and protease inhibitors. Solubilized membranes were clarified by centrifugation at 100,000 xg, and the supernatant was loaded onto a pre-equilibrated column of anti-DYKDDDDK G1 affinity resin (Genscript). The resin was washed with Buffer A (20 mM HEPES, pH7.5, 150 mM NaCl, 10 μM CGP55845, and protease inhibitors) with 0.1% DDM and 0.02% CHS. Protein was eluted with Buffer A containing 0.1% DDM, 0.02% CHS, and 0.2 mg/mL DYKDDDDK peptide. The eluate was then loaded onto a pre-equilibrated Nickel-NTA column. Resin was washed with Buffer A containing 0.1% DDM, 0.02% CHS; and the buffer was exchanged in six steps to Buffer A supplemented with 0.2% GDN, 0.02% CHS, followed by a two-step exchange into Buffer A containing 0.004% GDN, 0.0004% CHS. Protein was eluted from the Ni-NTA resin with Buffer A containing 0.004% GDN, 0.0004% CHS, and 500 mM Imidazole. The resulting eluate was concentrated by centrifugal filtration with a 50 kDa molecular weight cut off, and

subsequently run on a Superose 6 size exclusion column (GE Healthcare). Samples were pre-screened for sample quality by negative stain transmission electron microscopy and then immediately prepared on cryoEM grids.

CryoEM Data Collection

For the $GABA_{B1b}$/$GABA_{B2}$ heterodimer, 3.5 μL of sample was applied at a concentration of 3–5 mg/mL to glow-discharged holey carbon grids (Quantifoil R1.2/1.3). The grids were blotted using an FEI Vitrobot Mark IV (Thermo Fisher Scientific) at 18 °C and 100% humidity, and plunge frozen into liquid ethane. Two data sets were used to produce the final structure. For both data collections cryoEM imaging was performed on a Titan Krios (Thermo Fisher Scientific) electron microscope equipped with a K3 Summit direct electron detector (Gatan). The microscope was operated at 300 kV accelerating voltage, at a magnification of 57,050x in counting mode resulting in a magnified pixel size of 0.8521 Å. For the first data set, movies were obtained at an exposure rate of 14.19 electrons/ $Å^2$/sec with defocus ranging from −1.5 to −2.7 μm. The total exposure time was 3.985 sec over 57 frames per movie stack. For the second data set, movies were obtained at an exposure rate of 21.43 electrons/ $Å^2$/sec with defocus ranging from −1.2 to −2.5 μm. The total exposure time was 2.996 sec including 50 frames per movie stack.

CryoEM grids for the $GABA_{B1b}$ homodimer at a concentration 5.0 mg/mL were prepared similar to the heterodimer. CryoEM imaging was performed on a Titan Krios electron microscope equipped with a post-column energy filter and a K2 Summit direct electron detector (Gatan). The microscope was operated at 300 kV accelerating voltage, at a magnification of 47,198x in counting mode resulting in a pixel size of 1.06 Å. Movies were obtained at an exposure rate of 6.212 electrons/$Å^2$/sec with defocus ranging from −0.9 to −2.5 μm. The total exposure time was 8.0 sec over 40 frames per movie stack. Automatic data acquisition was performed using SerialEM[37] for all data sets.

Image Processing and 3D Reconstruction

Dose-fractionated image stacks were subjected to beam-induced motion correction and dose-weighting using MotionCor2[38]. Contrast transfer function parameters for each non-dose weighted micrograph were determined by Gctf[39] for the homodimer and data set #1 of the heterodimer, and by CtfFind-4.1[40] for data set #2 of the heterodimer. For all data sets; particle selection, 2D and 3D classification were performed on a binned dataset (pixel size 1.72Å and 4.24Å for the heterodimer and homodimer, respectively) using RELION (versions 3.0 and 3.1)[41]. The two data sets for the heterodimer were processed individually before being combined following a Bayesian polishing step. A total of 538,957 particles from 1,324 micrographs and 2,062,083 particles from 8,991 micrographs were extracted using semi-automated particle selection for the heterodimer data set #1 and #2, respectively. Both particle sets were then separately subjected to three rounds of 2D classification and two rounds of 3D classification. Particles in both sets were subjected to Bayesian polishing individually and then combined for a total of 286,140 particles. The merged dataset was fit for Ctf parameters (per particle defocus and astigmatism, per micrograph *B*-factor) and estimated for anisotropic magnification and beam-tilt. A final 3D refinement was followed by post-processing using a mask that excluded the GDN micelle density. A focused

refinement was also carried out using a mask encompassing the VFT and linker regions of $GABA_B$. For the $GABA_{B1b}$ homodimer structure, a total of 2,278,113 particles were extracted from 5,602 micrographs using semi-automated particle selection. Particles were subjected to multiple rounds of 2D and 3D classification until a subset of 282,811particles were selected for the final map. The particle set underwent multiple rounds of Ctf parameter fitting and was subjected to Bayesian polishing before 3D Refinement and post-processing of the final map. UCSF Chimera[42] was used for map/model visualization.

Model Building

The initial model for the VFT domain was taken from the inactive state VFT crystal structure PDB:4MR7[12] and the initial structure of the transmembrane domain of $GABA_{B1b}$ was generated as a homology model from the inactive cryoEM structure of mGlu5 (PDB:6N52, 38% sequence similarity to $GABA_{B1}$) using Schrödinger's Prime homology modeling[14]. Both components were placed into the $GABA_B$ cryoEM map using Chimera's 'fit-in-map' function. The linker, intracellular loops, and extracellular loops of $GABA_{B1}$ were interactively adjusted into the EM map using Coot (version 0.8.9.1el)[43] and the resulting model of the $GABA_{B1}$ Linker/7TM was then used to generate a homology model of $GABA_{B2}$ using Schrodinger's Prime homology modeling, which was also placed into the map in Chimera. Iterative rounds of interactive model adjustment in Coot followed by real-space refinement in Phenix (version 1.17.1–3660)[44] employing secondary structure restraints in addition to the default restraints were performed to improve the modeling. The resulting structure of $GABA_{B1}$ was sufficiently different than the original homology model such that that the RMSD between the homology model and the final model is non-trivial (~2.0Å in the transmembrane helices alone). Once confidence in the sidechain placement was reached for the ligand-binding cleft on $GABA_{B1}$, the GemSpot pipeline[17] (Schrödinger) was used to model the inhibitor, CGP55845, into the map. After further improvement, 1-palmitoyl-2-oleoyl-sn-glycero-3-phosphoethanolamine (POPE) was modeled in the transmembrane pocket of $GABA_{B1}$ and $GABA_{B2}$ with the GemSpot pipeline. Final refinement was performed with Phenix[44].

Molecular Dynamics Simulations and Analysis

To prepare the system for molecular dynamics simulations, the low-resolution features of the map were used to manually build ICL2 into the model of the $GABA_{B1}$/$GABA_{B2}$ inactive heterodimer using Coot. The system was then prepared in Maestro, version 2019–4 (Schrödinger) to build any stubbed sidechains and determine protonation states. The VFTs were removed from the heterodimer to produce a truncated construct starting at residues T461 for $GABA_{B1b}$ and T468 for $GABA_{B2}$, thus containing only the linkers and the TM domains. The Orientations of Proteins in Membranes (OPM)[45] webserver was used to orient the system with respect to a membrane plane and the CHARMM-GUI[46] was employed to generate a pdb of the system in either a 1-palmitoyl-2-oleoyl-sn-glycero-3-phosphocholine (POPC) and cholesterol bilayer or a 3:1 POPC:1-palmitoyl-2-oleoyl-sn-glycero-3-phosphoethanolamine (POPE) and cholesterol bilayer. Approximate dimensions for the system were 105 × 105 × 110 Å for a total of 240 lipid and 7 cholesterol molecules. This bilayer was then solvated in TIP3P water with 150 mM sodium chloride ions balanced to achieve charge neutrality. The salt concentration of 150 mM is consistent with the conditions

at which the receptor was purified. POPE was used for the lipid in the TM binding sites of $GABA_{B1}$ and $GABA_{B2}$.

The PDB file for the full solvated system was prepared in VMD (version 1.9.3)[47] for simulation in NAMD (version 2.13)[48] to produce a protein structure file (psf). The OPLS-AA/M[49] force field was used for the protein, while OPLS-AA[49] was used for the lipids, cholesterol, and ions. Disulfide bonds were placed between C546 and C644 in $GABA_{B1}$ and C553 and C648 in $GABA_{B2}$ and both the N- and C- termini were blocked with capping groups, acetylated N-termini, and N-methylamide C-termini. NAMD was used to run molecular dynamics simulations, where all phases employed periodic boundary conditions with non-bonded interactions smoothed starting at 10 Å to 12 Å, with long range interactions treated with the particle mesh Ewald method. Systems were minimized for 2000 steps and then slowly heated in the NPT ensemble with a Langevin thermostat and a Nosé-Hoover Langevin piston barostat set at 1 atm with a period of 50 fs and a decay of 25 fs. A 2 fs time-step was used with the SHAKE[50] and SETTLE[51] algorithms. Heating occurred from 0 K to 310 K in increments of 20 K with 0.4 ns of simulation at each increment. Harmonic restraints of 1 kcal/mol/$Å^2$ were used during heating on all non-hydrogen atoms of the protein and lipids. The system was then equilibrated with 1 kcal/mol/$Å^2$ harmonic restraints on all protein and lipid non-hydrogen atoms for 10 ns followed by another 10 ns of equilibration with 1 kcal/mol/$Å^2$ harmonic restraints on non-hydrogen backbone atoms. Finally, 1 kcal/mol/$Å^2$ harmonic restraints were applied to only C alpha atoms for 2 ns before being stepped down to 0.5 kcal/mol/$Å^2$ for 2 ns, 0.3 kcal/mol/$Å^2$ for 2 ns, and then removed. The first 30 ns of unrestrained molecular dynamics were also discarded as equilibration.

All trajectories were down sampled by 10x for analysis. Cavity volume was calculated with Epock (1.0.5)[52] in VMD[47] on trajectories that had been aligned to either $GABA_{B1}$ or $GABA_{B2}$ from the starting structure. The cavity region was defined to include the binding region of the hydrophobic tails of the lipid. TM-TM distances were calculated in VMD based on the CA position of residues: 3.33, 4.50, 5.40, 6.54, and 7.28 in the Ballesteros–Weinstein[53] numbering scheme.

Transfection and seeding of cells for signaling assays

HEK293 cells (ATCC® CRL-1573™) were transfected with expression vector DNAs encoding the two $GABA_B$ receptor protomers and a chimeric $G\alpha_{q/o5}$ subunit (five C-terminal amino acids of $G\alpha_q$ were exchanged with those of $G\alpha_o$) to allow the $G\alpha_{i/o}$-coupled $GABA_B$ receptor to activate PLC and induce IP_3 and intracellular Ca^{2+} release[3]. Prior to transfection cells were brought into suspension by trypsinization and resuspension to 0.18 million cells/mL in growth medium (D-MEM, Gibco 10566016; supplemented with 10% Fetal Bovine Serum, Gibco 10270106; 1% Sodium Pyruvate, Gibco 11360039; 1% MEM Non Essential Amino Acids, Gibco 11140068; and 1% Penicillin-Streptomycin Solution, Gibco 15140122).

For each 1 mL of cell suspension transfected, a total of 1 μg DNA in 25 μL OptiMEM (Gibco 51985) was incubated for 20 min with a mixture of 57 μL OptiMEM and 3 μL FuGene6 (Promega E2692). After FuGene6/DNA complex formation, the mixture was

added directly to the cell suspension, mixed thoroughly and cells seeded with 100 μL cell suspension in appropriate 96-well plates. Of the 1 μg DNA/mL cell suspension, the amount of expression vector DNA encoding the chimeric $G\alpha_{q/o5}$ was 0.5 μg/mL cell suspension in all experiments. The amount of $GABA_B$ encoding DNA was varied between 7.8 ng and 0.25 μg for each of the $GABA_B$ receptor protomer DNAs depending on the assay and mutants tested. Empty vector DNA was added to give a total amount of 1 μg DNA/mL cell suspension transfected. For characterization of basal activity of the TM3/5 protomer mutants, a typical gene dose experiment was performed. DNA corresponding to 62.5 ng DNA/mL cell suspension of each of the protomers (wild-type or mutants) were mixed and serially diluted 2-fold 5 times, typically down to 3.9 ng DNA/mL cell suspension. The transfected cell suspension was seeded at 100 μg/mL both in clear poly-L-lysine coated 96-well plates for IP_1 accumulation assays and in white poly-L-lysine coated 96-well plates for cell surface ELISA assays.

IP_1 accumulation assays

The IP_1 assays for wild-type and mutant receptors was performed essentially as described[14]. Forty-eight hours after transfection, the growth medium was replaced with HBSS buffer (HBSS (Gibco 14025), 20 mM HEPES pH 7.5, 1 mM $CaCl_2$, 1 mM $MgCl_2$ and 0.1% BSA) supplemented with BSA to 0.5% and incubated at 37 °C for 3–4 hours.

For characterization of the TM3/TM5 protomer interface mutants for basal activity, the HBSS + 0.5% BSA buffer was replaced with 100 μL HBSS buffer, followed by addition of 50 μL HBSS buffer containing LiCl (150 mM) to give a final concentration of 50 mM LiCl. After incubation for 1 hour at 37°C the IP_1 accumulation was stopped by addition of 40 μL CisBio IP-One Tb HTRF Kit (CisBio, 62IPAPEC) lysis buffer. The accumulated IP_1 levels were determined according to the manufacturer's instructions and as described[14].

For the generation of GABA concentration response curves, the compounds were diluted in three times the final concentration in HBSS buffer containing 60 mM LiCl. The assay was started, first by replacing the HBSS + 0.5% BSA buffer with 100 μL HBSS buffer, followed by addition of 50 μL of the above compound dilutions to give a final LiCl concentration of 20 mM. The IP_1 accumulation assay was stopped and assayed as described above after incubation for 1 hour at 37 °C. Data were calculated as the amount of IP_1 formed per well or normalized to the basal IP_1 level and fitted by non-linear regression using GraphPad Prism. Results and description of statistical analyses used in this manuscript are found in Supplementary Information Table 1.

Cell surface ELISA assay

Surface expression levels of wild-type and mutant $GABA_B$ receptors were determined using a direct enzyme-linked immunosorbent assay (ELISA) against the N-terminal $GABA_{B1b}$ FLAG tag and the N-terminal $GABA_{B2}$ HA-tag, as described[54]. Transfected cells were seeded in white Poly-D-Lysine-coated 96-well plates. Forty-eight hours after transfection, cells were washed once with 100 μL/well DPBS + 1 mM $CaCl_2$ (wash buffer). Following fixation with 50 μL/well 4% paraformaldehyde solution for 5 minutes at room temperature, cells were washed twice with 100 μl wash buffer and blocked with 100 μL/well blocking

solution (3% dry-milk, 1 mM $CaCl_2$, 50 mM Tris-HCl, pH 7.5) for 30 minutes at room temperature, followed by addition of 75 μL/well HRP-conjugated anti-FLAG antibody (Sigma Aldrich, A8592), or HRP-conjugated anti-HA antibody (R&D systems HAM0601), both diluted 1:2000 in blocking solution, and allowed to incubate for 1 hour at room temperature. The plates were then washed four times with 100 μl/well blocking solution followed by four washes with wash buffer. The amount of surface expressed receptors was detected by adding 60 μL wash buffer and 20 μL HRP substrate (Bio-Rad, 170–5060) per well, incubating for 10 minutes and measuring of luminescence in an EnVision plate reader (Perkin Elmer).

Statistics and Reproducibility

Detailed results and description of statistical analyses used in this manuscript are found in Supplementary Table 1. Data and error bars in Figs. 1c and 1d represent mean ± S.E.M. from at least five independent experiments. In Fig. 1c, data of co-expressed $GABA_{B1}$-WT (6.3 ng) with $GABA_{B2}$-WT (6.3 ng), $GABA_{B1}$-WT (3.1 ng) with $GABA_{B2}$-WT (3.1 ng), and $GABA_{B1}$-WT (1.6 ng) with $GABA_{B2}$-WT (1.6 ng) represent n=7 independent experiments; data of co-expressed $GABA_{B1}$-WT (0.8 ng) with $GABA_{B2}$-WT (0.8 ng), solely expressed $GABA_{B1}$-WT (6.3 ng), solely expressed $GABA_{B2}$-WT (3.1 ng), and untransfected HEK293 cells represent n=6 independent experiments. In Fig. 1d, data of co-expressed $GABA_{B1}$ (Δ627–634) with $GABA_{B2}$-WT, and $GABA_{B1}$-WT with $GABA_{B2}$ (Δ631–638) represent n=7 independent experiments; and co-expressed $GABA_{B1}$ (Δ627–634) with $GABA_{B2}$ (Δ631–638) represent n=5 independent experiments. Data in Fig. 2d are representative of one experiment performed in triplicate and repeated independently at least three times with similar results (n=3), data points and error bars represent mean ± S.E.M. Data in Fig. 2e represent mean ± S.E.M. from at least three independent experiments; data for co-expressed $GABA_{B1}$ (H572A/E673A) with $GABA_{B2}$-WT, and $GABA_{B1}$-WT with $GABA_{B2}$ (H579A/E677A) represent n=3 independent experiments; and data for $GABA_{B1}$-WT with $GABA_{B2}$-WT represent n=7 independent experiments. Data in Fig. 3d represent mean ± S.E.M. from at least four independent experiments; co-expressed $GABA_{B1}$ (L553W) with $GABA_{B2}$ (L560W) represent n=5 independent experiments, and $GABA_{B1}$ (R549A) with $GABA_{B2}$ (R556A) represent n=4 independent experiments, and data for $GABA_{B1}$-WT with $GABA_{B2}$-WT represent n=7 independent experiments. Ensemble data in Fig. 3e represent distribution over a 200 ns time course, for 5 simulations per condition, each violin represents n=37,500 time points.

Extended Data

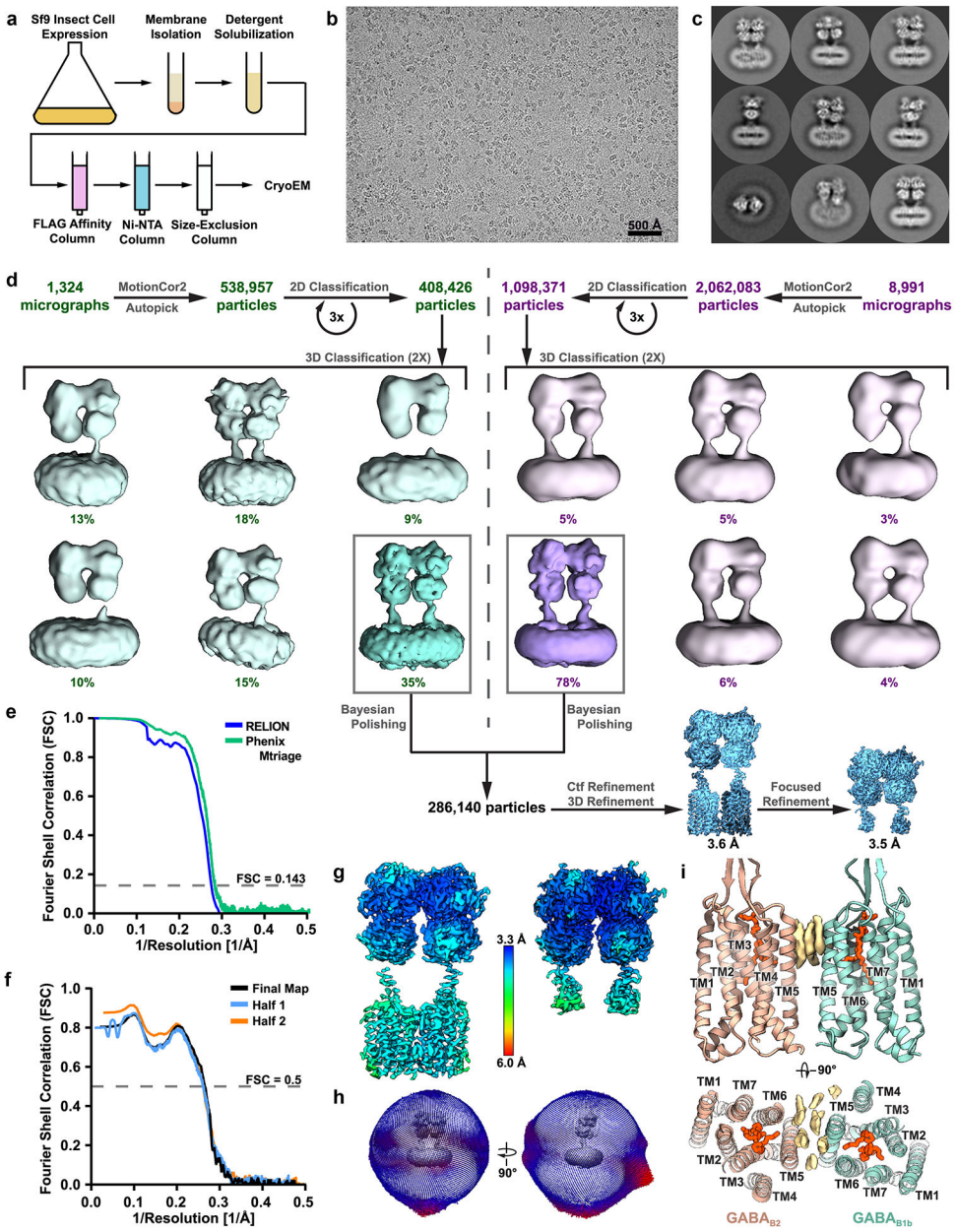

Extended Data Figure 1. Sample preparation, cryoEM processing and reconstruction of GABA$_B$ heterodimer.

a, Purification scheme for GABA$_B$. Representative cryoEM micrograph of 10,315 collected (**b**) and 2D class averages (**c**) of GABA$_B$ dimers. **d**, Flow chart outlining the cryoEM processing workflow using RELION[56], the global resolutions of the full-length structure and VFT focused structures were 3.6 Å and 3.5 Å, respectively, at 0.143 Fourier shell correlation (FSC) as calculated by RELION. **e**, **f**, Gold standard FSC curve of half-maps calculated using RELION and Phenix Mtriage[57] (**e**), and map-to-model validation curves generated through Phenix Mtriage (**f**). **g**, Local resolution of cryoEM maps. **h**, Angular distribution of projections used in final cryoEM reconstruction. **i**, Ordered cryoEM densities (light yellow),

likely corresponding to GDN and/or cholesteryl hemisuccinate, are found at the TM5 interface of $GABA_{B1}$ and $GABA_{B2}$ 7TM domains.

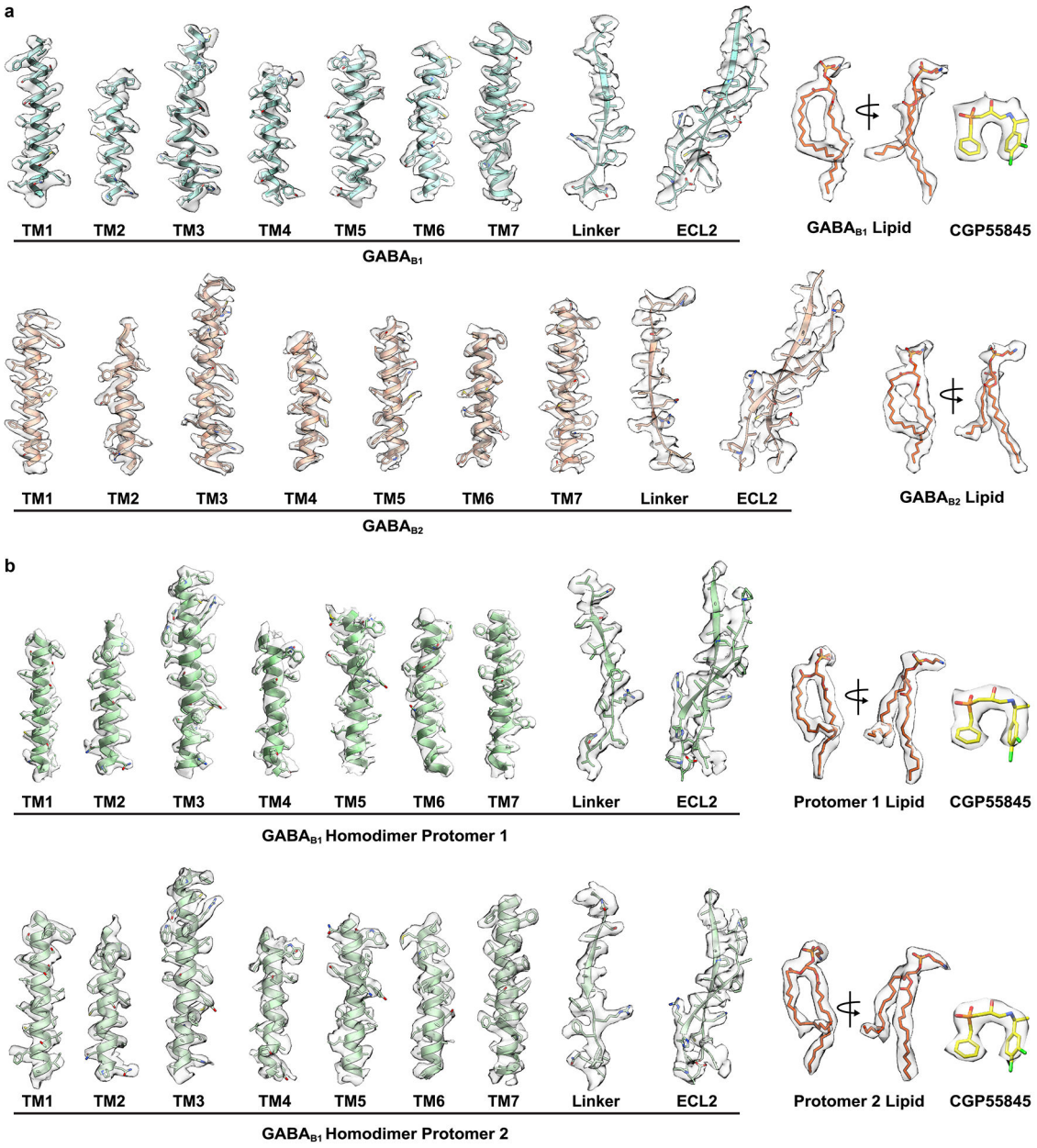

Extended Data Figure 2. Agreement between cryoEM map and model.

a, EM density and model for $GABA_B$ heterodimer complex; transmembrane helices of $GABA_{B1}$, transmembrane helices of $GABA_{B2}$, linker region, bound PE, and ligand CGP55845. Densities visualized within UCSF Chimera[42] and zoned at 2.2 with threshold set to 0.0142, with the exception of the following: $GABA_{B1}$-bound lipid,$GABA_{B1}$-bound CGP55845, and $GABA_{B2}$ linker in which thresholds of 0.01, 0.0189, and 0.0127 were used, respectively. **b**, EM density and model for $GABA_{B1}$ homodimer; transmembrane helices and linker region of both protomers, 7TM-bound PE, and ligand CGP55845. Densities were zoned at 2.2 and threshold set to 0.016, apart from CGP55845 and the ECL2 in both protomers in which a threshold of 0.03 or 0.02 was used, respectively.

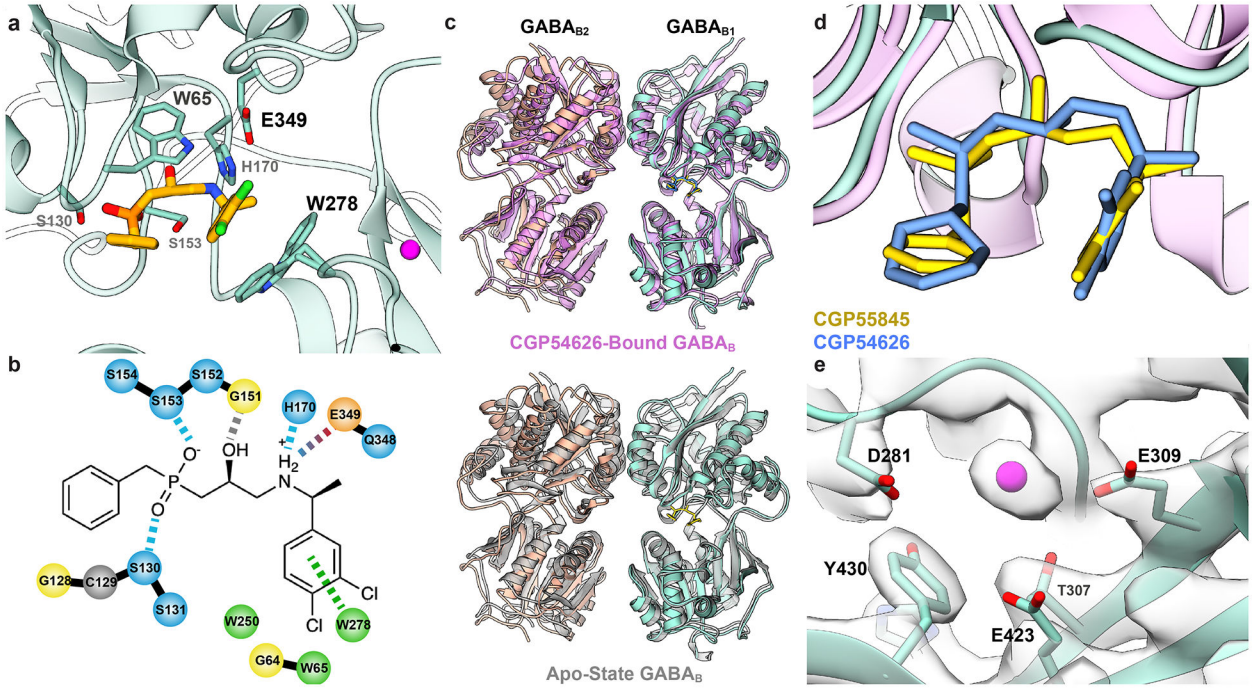

Extended Data Figure 3. Binding of CGP55845 and cation to GABA$_{B1}$ VFT domain.

a, Model of CGP55845 within the VFT of GABA$_{B1b}$. The entire ligand is confined by W65 and W278 of GABAB1 that form hydrophobic interactions with the chlorinated ring of CGP55845. **b**, Schematic of interacting residues on GABA$_{B1b}$ with the inhibitor, CGP55845. GABA$_{B1b}$ residues S153 and S130 form hydrogen bonds with oxygen atoms of the phosphate group, while H170 and E349 form a hydrogen bond and a salt bridge with the amine group of the ligand, respectively. **π-π** stacking occurs between the chlorinated ring structure of CGP55845 and W278, while W65 provides hydrophobic packing on the opposing side of the ring. S130, H170, E349, and W65 are all substantially different residues in GABA$_{B2}$, precluding ligand binding. Residues are color-coded corresponding to their properties: light blue, hydrophilic; orange, anionic; green, hydrophobic; yellow, glycine; and grey, cysteine. Interaction lines are also color-coded according to their type: light blue, side-chain hydrogen bonding; grey, backbone hydrogen bonding; blue-red gradient, salt-bridge; and green, **π-π** stacking. **c**, Overlay of CGP55845-bound GABA$_B$ cryoEM structure (tan/teal) with CGP54626-bound GABA$_B$ crystal structure (pink, PDB:4MR7) or apo-state GABA$_B$ crystal structure (grey, PDB:4MQE), resulting in RMSD values of 1.30 Å and 1.28 Å respectively[12]. **d**, Comparison of ligand pose between CGP55845 (yellow) and CGP54626 (blue) , which differs from CGP55845 only in a substitution of an aromatic ring in place of cyclohexane. **e**, Spherical density surrounded by anionic residues within the VFT supports a cation (magenta) at that site. The presence of a metal ion would be consistent with the observation that calcium and other divalent ions affect ligand affinity[58,59], and examination of the deposited scattering factors for the high-resolution VFT crystal structure (PDB:4MR7) reveals positive difference density also consistent with a cation at this site[12].

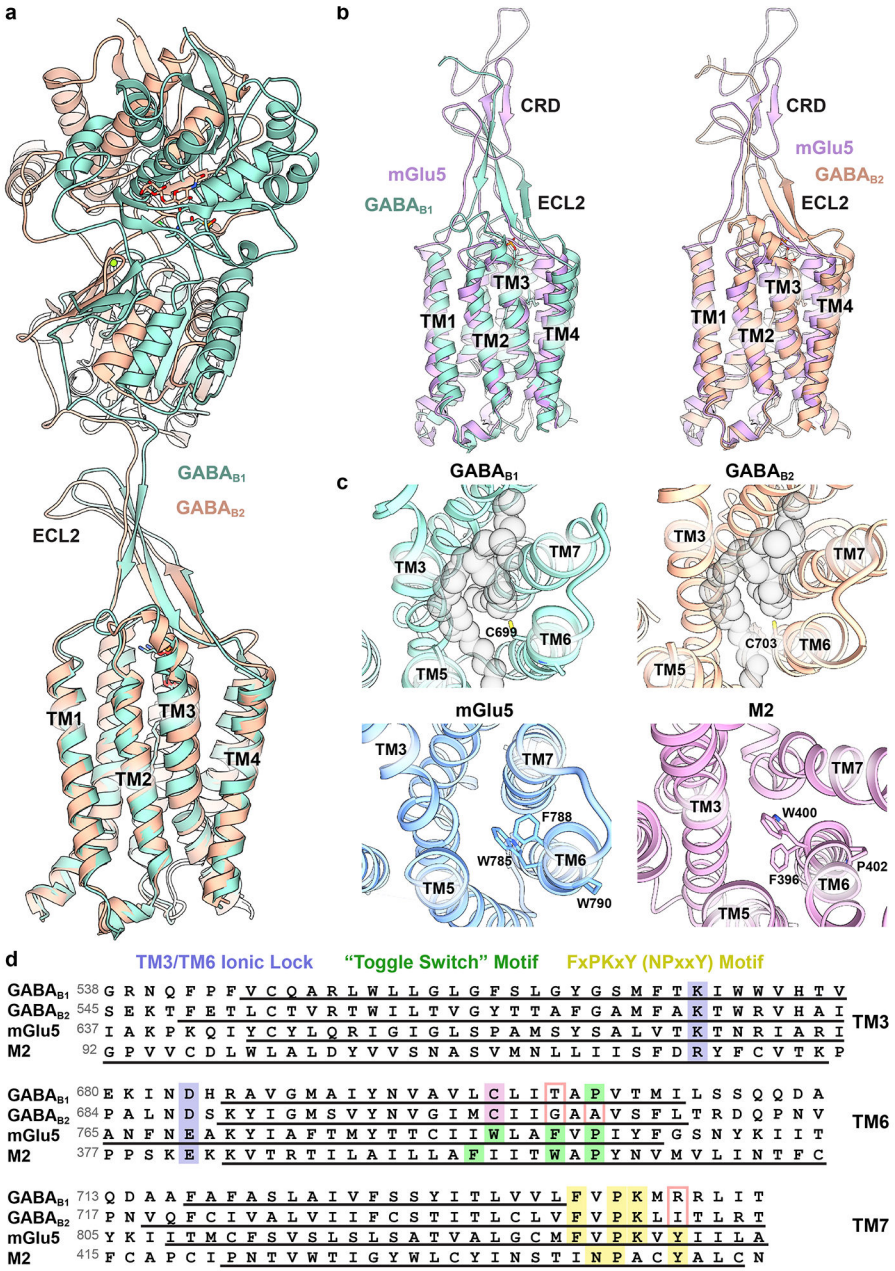

Extended Data Figure 4. Comparison of structures across GPCR classes.

a, GABA$_B$ protomers share similar secondary and overall structure. **b**, Comparison of mGlu5 and GABA$_B$ 7TM and ECL2/linker shown from side view. **c**, Top-down view of GABA$_{B1}$, GABA$_{B2}$, mGlu5 (PDB: 6N52), and class A M2 acetylcholine receptor (PDB:3UON) with sidechains corresponding to the "toggle-switch" motif shown. Phospholipid space-filling model is included in gray within GABA$_{B1}$ and GABA$_{B2}$. **d**, Sequence alignment of human GABA$_B$ receptors with mGlu5 and M2 receptors comparing canonical GPCR activation motifs: TM3-TM6 ionic lock (blue), "toggle switch motif" (green), FxPKxY motif (yellow). Sequences are aligned to motifs within each TM helix and transmembrane helical secondary structure is underlined. Residues in GABA$_B$ sequences

differing from canonical motifs are outlined in pink. The cysteine residue that replaces the “toggle-switch” tryptophan is highlighted in pink.

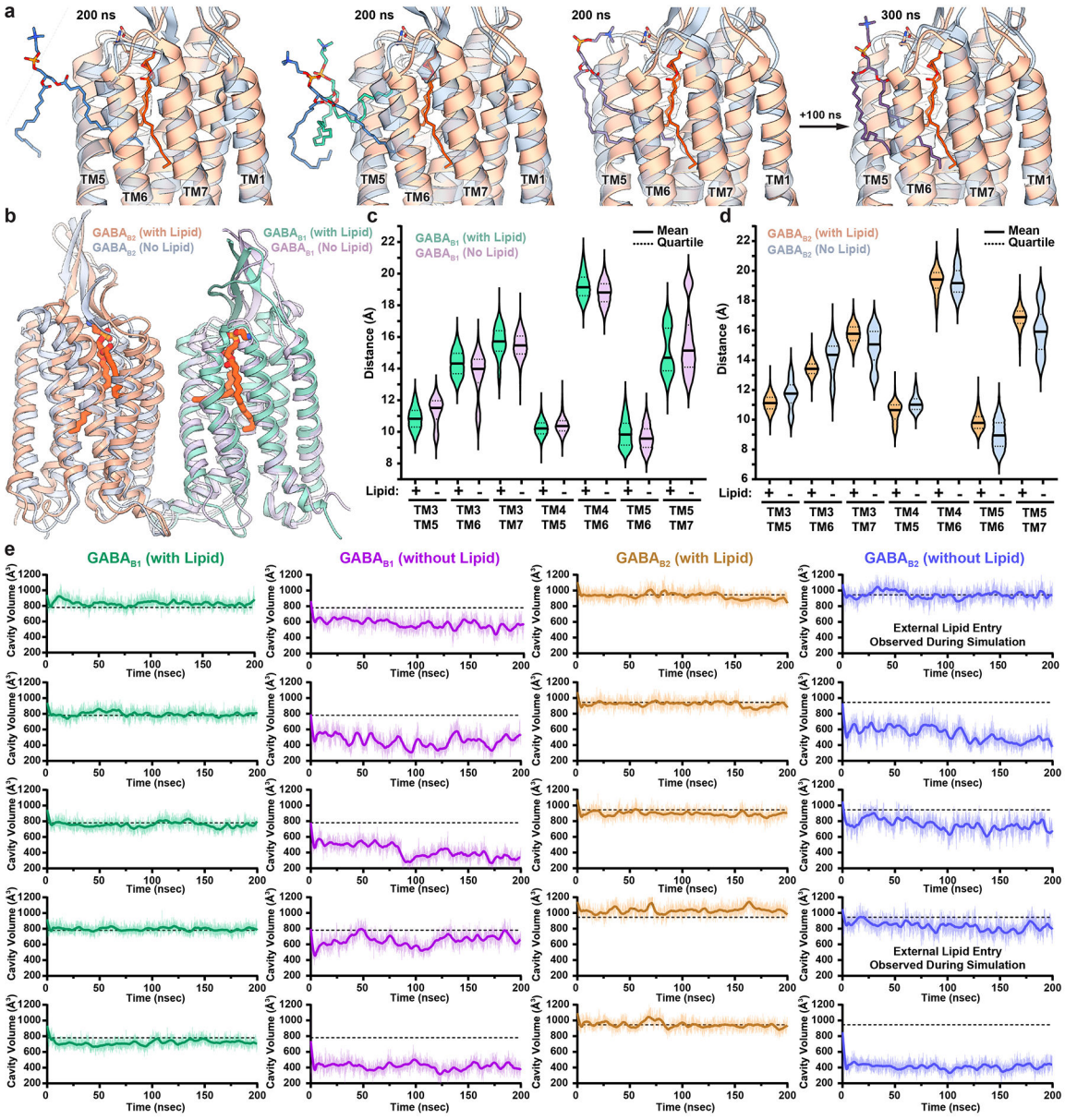

Extended Data Figure 5. Atomistic simulations of phospholipid structural stabilization and entry.

a, The results of three out of seven total simulations of $GABA_B$ 7TM and linker in the absence of core-bound lipid after 200 ns. The results show the extent of lipid (green, purple) entry in $GABA_{B2}$ (grey) in the simulations versus the experimental structure (tan) with PE (orange). One of the trajectories was extended an additional 100 ns (rightmost panel) and lipid entry was observed to progress towards the core. **b**, Representative side view of the $GABA_B$ ribbon and stick model from simulations at 200 ns showing persistence of the ECL2/β-sheet structure even in absence of VFT domains. **c**, **d**, Violin plots of ensemble distances between $GABA_{B1}$ (**d**) and $GABA_{B2}$ (**e**) TM helices in simulations with and without core-bound lipid. Distances were measured from the Cα atoms of the following residues in $GABA_{B1}$: L550 (TM3), W611 (TM4), L653 (TM5), M707 (TM6), A716 (TM7);

and the following residues in $GABA_{B2}$: T557 (TM3), W615 (TM4), L657 (TM5), F711 (TM6), Q720 (TM7). Simulations were run over 200 ns and violin plots represent n=37,500 data points and 5 simulations per condition. **e**, 7TM cavity volume measured over time for individual simulations. Average cavity volume of phospholipid-bound receptor is shown as dashed line, thick lines indicate rolling averages of 5.33 ns, and thin lines represent raw data.

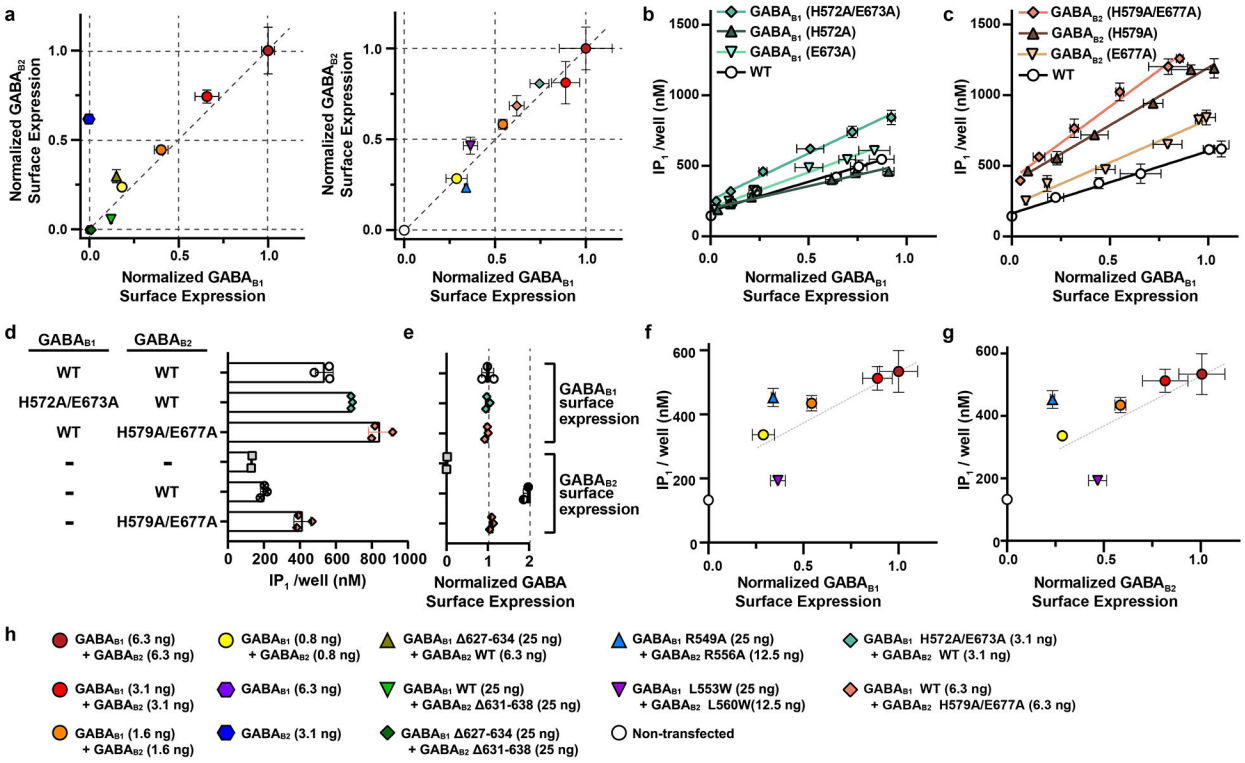

Extended Data Figure 6. Functional analysis of GABA$_B$ mutants.

a, Comparative normalized surface expression levels of constructs. Surface expression levels of wild-type and mutant GABA$_B$ receptors were determined using a direct enzyme-linked immunosorbent assay (ELISA) against the N-terminal GABA$_{B1}$ FLAG tag and the N-terminal GABA$_{B2}$ HA-tag. Surface expression levels were normalized to the surface expression of a wild type GABA$_B$ receptor when 6.3 ng FLAG-tagged GABA$_{B1}$ and 6.3 ng HA-tagged GABA$_{B2}$ DNA was used for transfection. The line x=y indicates similar surface expression of GABA$_B$ subunits as evident from transfection with lower amounts of FLAG-tagged GABA$_{B1}$ and HA-tagged GABA$_{B2}$. Values above the line have greater GABA$_{B2}$ surface expression relative to GABA$_{B1}$ and values below the line have greater GABA$_{B1}$ surface expression relative to GABA$_{B2}$. GABA$_{B1}$ did not reach the cell surface (data point hidden behind triangle at the coordinate (0,0) in the left subpanel). **b**, **c**, Mutations of ionic residues forming the interface of GABA$_{B1}$ (**b**) and GABA$_{B2}$ (**c**) result in increased constitutive activity of the receptor. To achieve a range of expression levels of the mutants in b and c, the DNA amounts transfected were serially diluted 2-fold from 3.3 ng (panel b mutants) or 6.3 ng (panel c mutants) of each subunit, respectively. **d**, GABA$_{B2}$ H579A/E677A expressed without GABA$_{B1}$ shows a moderate increase in basal activity over wild-type GABA$_{B2}$ expressed alone, although surface expression (**e**) of the wild-type GABA$_{B2}$ subunit was higher than of GABA$_{B2}$ H579A/E677A. **f**, **g,** Mutation of lipid coordinating residues (blue triangle) increase the constitutive activity of GABA$_{B1}$ (**f**) and GABA$_{B2}$ (**g**), while mutations displacing the lipid tails from the 7TM core (purple triangle) result in decreased basal activity of the receptor when compared to wild-type receptor of similar receptor surface expression. **h**, Key to colors and symbols used in panels **a**, **f**, and **g** with DNA transfection amounts indicated in parenthesis. Data are representative of one

experiment performed in triplicate and repeated independently at least three times with similar results (n=3 independent experiments), error bars represent mean ± S.E.M.

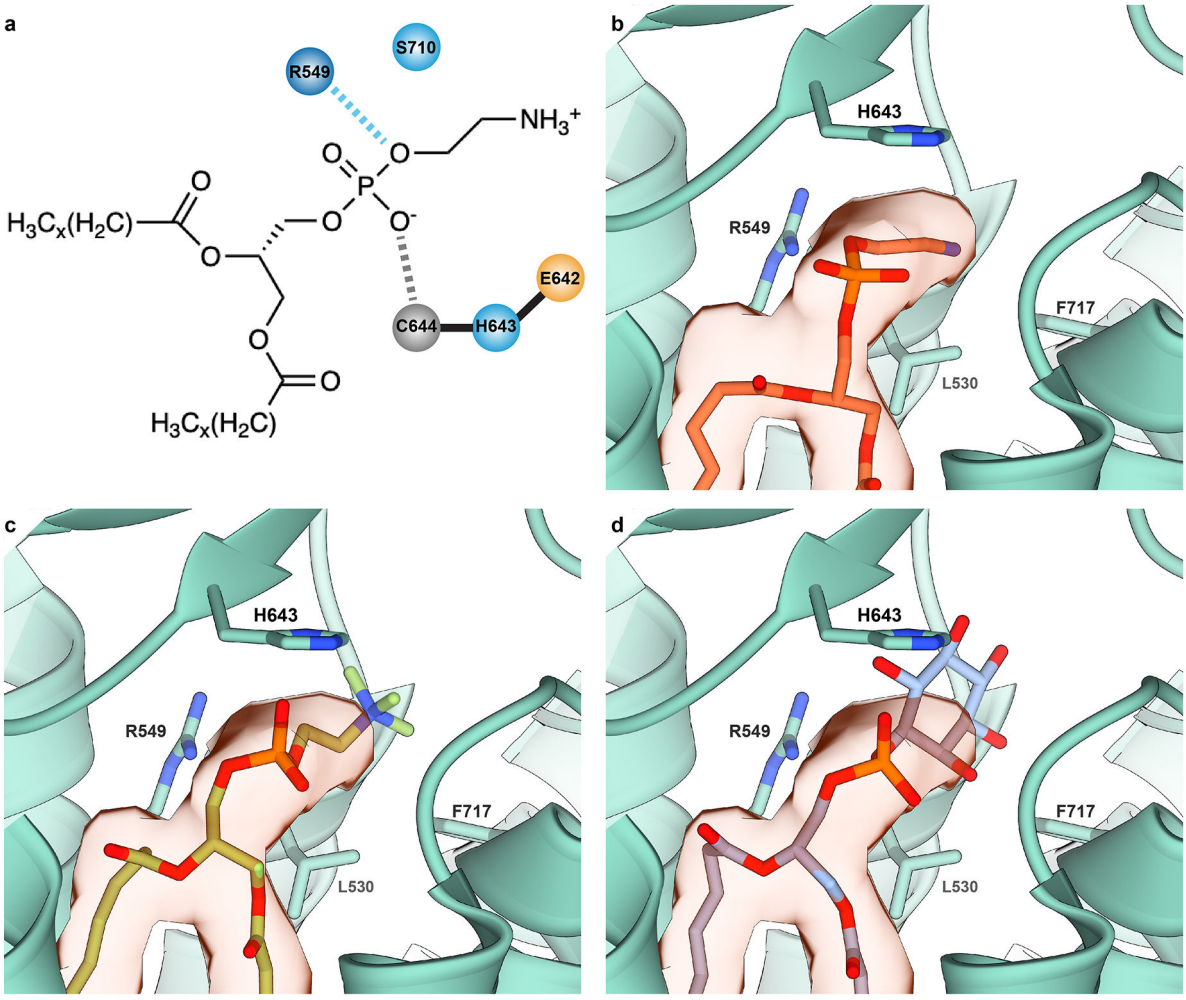

Extended Data Figure 7. Modeling of phospholipid into $GABA_B$.

a, Schematic of $GABA_{B1}$ residues interacting with the polar headgroup of phosphatidylethanolamine (PE). The terminal amine (-NH^{3+}) forms a salt bridge with residue $D714^{ECL3}$, while the phosphate group is coordinated by $S710^{ECL3}$, $R549^{TM3}$, and the backbone nitrogen of $C644^{ECL2}$. **b-d**, As our receptor purification did not contribute additional lipid, we considered the known lipid composition of Sf9 insect cells. Four primary phospholipids are present in Sf9 insect cells: phosphatidylcholine (43%), phosphatidylethanolamine (32%), phosphatidylinositol (23%), and cardiolipin (4%)[60]. It was apparent from the map that the lipid had only two carbon chains, immediately excluding cardiolipin as it has four hydrocarbon tails. A comparison of the map and the binding site residues led to the decision to model PE (**b**) into the pocket using the GemSpot pipeline[17], which produced good cross-correlation with favorable interactions. To further confirm our selection, analysis of overlays of phosphatidylcholine (**c**) and phosphatidylinositol (**d**) over the docked model revealed phosphatidylcholine is unlikely given that the interactions with the cation appear to be primarily salt bridges, rather than the cation-**π** interactions that more commonly coordinate choline in proteins[61]. Although phosphatidylinositol may make favorable interactions, our map does not appear to support such a large moiety in the

headgroup position. Thus, PE is the most likely lipid to reside in the structure and was therefore used in the models.

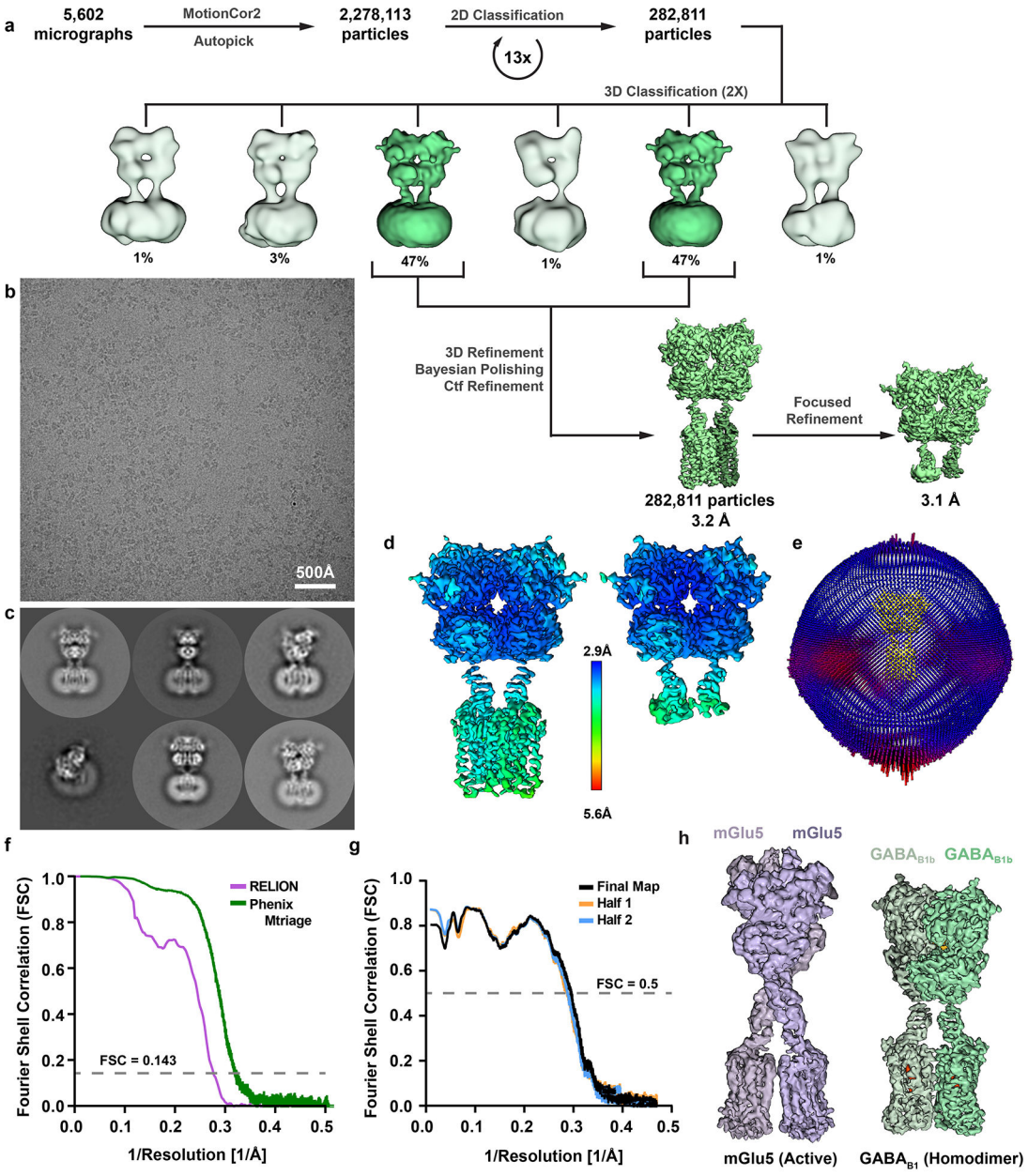

Extended Data Figure 8. CryoEM processing workflow of GABA$_{B1b}$ homodimer.

a, Flow chart outlining the cryoEM processing of the GABA$_B$ homodimer. **b**, **c**, Representative micrograph of 5,602 collected (**b**) and 2D class averages (**c**). **d**, Local resolution of cryoEM maps. **e,** Angular distribution of projections employed in the final cryoEM reconstruction. **f**, **g**, Gold standard FSC curve of half-maps calculated using RELION and Phenix Mtriage[57] (**f**), and map-to-model validation curves generated through Phenix Mtriage (**g**). Global indicated resolutions of the full-length structure and VFT structure were 3.2 Å and 3.1 Å, respectively, at 0.143 Fourier shell correlation (FSC) as calculated by RELION. **h,** EM maps of active mGlu5 (purple, EMD-0345), and homodimeric GABA$_{B1}$ (green). The GABA$_{B1}$ homodimer adopts a similar overall architecture as active mGlu5.

Extended Data Table 1.

Cryo-EM data collection, refinement, and validation statistics.

	$GABA_{B1b}/GABA_{b2}$ Heterodimer (EMDB-21533) (PDB-6W2X)		GABAB1b Homodimer (EMDB-21534) (PDB-6W2Y)
Data collection and processing	Data Set #1	Data Set #2	
Magnification (x)	57,050	57,050	47,198
Voltage (kV)	300	300	300
Electron exposure (e−/Å^2)	56.5	64.2	49.7
Defocus range (nm)	−1.5 – −2.7	−1.2 – −2.5	−0.9 – −2.5
Pixel size (Å)	0.8521	0.8521	1.06
Symmetry imposed	C1	C1	C1
Initial particle images (no.)	538,957	2,062,083	2,278,113
Final particle images (no.)	286,140 (Combined Data Sets)		282,811
Map resolution (Å)	3.6 Å		3.2 Å
FSC threshold	0.143		0.143
Map resolution range (Å)	3.3 – 4.4		3.0 – 4.4
Map sharpening *B* factor (Å^2)	−183.273		−84.088
Refinement			
Initial model used (PDB code)	4MR7, 6N52 Homology		$GABA_{B1b}$ of 6W2X (this work)
Model resolution (Å)	3.7		3.4
FSC threshold	0.5		0.5
Model composition			
Non-hydrogen atoms	9860		9721
Protein residues	1345		1327
Ligands	3		4
B factors (Å^2)			
Protein	15.17		57.57
Ligand	28.97		59.82
R.m.s. deviations			
Bond lengths (Å)	0.004		0.007
Bond angles (°)	0.608		0.763
Validation			
MolProbity score	1.75		2.02
Clashscore	5.55		9.98
Poor rotamers (%)	0.00		0.12
Ramachandran plot			
Favored (%)	92.92		91.66
Allowed (%)	7.08		8.34
Disallowed (%)	0.00		0.00

Supplementary Material

Refer to Web version on PubMed Central for supplementary material.

Acknowledgements

The work is supported by National Institutes of Health (NIH) grant R01 NS092695 (G.S. and J.M.M.) and used the Extreme Science and Engineering Discovery Environment (XSEDE)[55] resource comet-gpu through sdsc-comet allocation TG-MCB190153, which is supported by National Science Foundation grant number ACI-1548562. We thank Qianhui Qu for advice and assistance with cryoEM.

References

1. Bettler B, Kaupmann K, Mosbacher J & Gassmann M Molecular structure and physiological functions of GABA(B) receptors. Physiological reviews 84, 835–867, doi:10.1152/physrev.00036.2003 (2004). [PubMed: 15269338]
2. Mannoury la Cour C, Herbelles C, Pasteau V, de Nanteuil G & Millan MJ Influence of positive allosteric modulators on GABA(B) receptor coupling in rat brain: a scintillation proximity assay characterisation of G protein subtypes. J Neurochem 105, 308–323, doi:10.1111/j.1471-4159.2007.05131.x (2008). [PubMed: 18021295]
3. Franek M et al. The heteromeric GABA-B receptor recognizes G-protein alpha subunit C-termini. Neuropharmacology 38, 1657–1666, doi:10.1016/s0028-3908(99)00135-5 (1999). [PubMed: 10587081]
4. Robbins MJ et al. GABAB2 Is Essential for G-Protein Coupling of the GABAB Receptor Heterodimer. The Journal of Neuroscience 21, 8043–8052, doi:10.1523/jneurosci.21-20-08043.2001 (2001). [PubMed: 11588177]
5. Galvez T et al. Mutagenesis and modeling of the GABAB receptor extracellular domain support a venus flytrap mechanism for ligand binding. J Biol Chem 274, 13362–13369, doi:10.1074/jbc.274.19.13362 (1999). [PubMed: 10224098]
6. Hepler JR & Gilman AG G proteins. Trends Biochem Sci 17, 383–387, doi:10.1016/0968-0004(92)90005-t (1992). [PubMed: 1455506]
7. Enna SJ GABAB receptor agonists and antagonists: pharmacological properties and therapeutic possibilities. Expert Opinion on Investigational Drugs 6, 1319–1325, doi:10.1517/13543784.6.10.1319 (1997). [PubMed: 15989503]
8. Malcangio M GABAB receptors and pain. Neuropharmacology 136, 102–105, doi:10.1016/j.neuropharm.2017.05.012 (2018). [PubMed: 28504122]
9. Pin JP, Galvez T & Prezeau L Evolution, structure, and activation mechanism of family 3/C G-protein-coupled receptors. Pharmacology & therapeutics 98, 325–354, doi:10.1016/s0163-7258(03)00038-x (2003). [PubMed: 12782243]
10. Brauner-Osborne H, Wellendorph P & Jensen AA Structure, pharmacology and therapeutic prospects of family C G-protein coupled receptors. Curr Drug Targets 8, 169–184, doi:10.2174/138945007779315614 (2007). [PubMed: 17266540]
11. Chun L, Zhang WH & Liu JF Structure and ligand recognition of class C GPCRs. Acta Pharmacol Sin 33, 312–323, doi:10.1038/aps.2011.186 (2012). [PubMed: 22286915]
12. Geng Y, Bush M, Mosyak L, Wang F & Fan QR Structural mechanism of ligand activation in human GABA(B) receptor. Nature 504, 254–259, doi:10.1038/nature12725 (2013). [PubMed: 24305054]
13. Geng Y et al. Structural mechanism of ligand activation in human calcium-sensing receptor. eLife 5, doi:10.7554/eLife.13662 (2016).
14. Koehl A et al. Structural insights into the activation of metabotropic glutamate receptors. Nature 566, 79–84, doi:10.1038/s41586-019-0881-4 (2019). [PubMed: 30675062]
15. Margeta-Mitrovic M, Jan YN & Jan LY A Trafficking Checkpoint Controls GABAB Receptor Heterodimerization. Neuron 27, 97–106, doi:10.1016/S0896-6273(00)00012-X (2000). [PubMed: 10939334]
16. Mukherjee RS, McBride EW, Beinborn M, Dunlap K & Kopin AS Point mutations in either subunit of the GABAB receptor confer constitutive activity to the heterodimer. Molecular pharmacology 70, 1406–1413, doi:10.1124/mol.106.024463 (2006). [PubMed: 16847143]

17. Robertson MJ, van Zundert GCP, Borrelli K & Skiniotis G GemSpot: A Pipeline for Robust Modeling of Ligands into Cryo-EM Maps. Structure (London, England : 1993), doi:10.1016/j.str.2020.04.018 (2020).
18. Conklin BR, Farfel Z, Lustig KD, Julius D & Bourne HR Substitution of three amino acids switches receptor specificity of Gq alpha to that of Gi alpha. Nature 363, 274–276, doi:10.1038/363274a0 (1993). [PubMed: 8387644]
19. Trinquet E et al. D-myo-inositol 1-phosphate as a surrogate of D-myo-inositol 1,4,5-tris phosphate to monitor G protein-coupled receptor activation. Analytical biochemistry 358, 126–135, doi:10.1016/j.ab.2006.08.002 (2006). [PubMed: 16965760]
20. Liu J et al. Molecular determinants involved in the allosteric control of agonist affinity in the GABAB receptor by the GABAB2 subunit. The Journal of biological chemistry 279, 15824–15830, doi:10.1074/jbc.M313639200 (2004). [PubMed: 14736871]
21. Audet M & Stevens RC Emerging structural biology of lipid G protein-coupled receptors. Protein science : a publication of the Protein Society 28, 292–304, doi:10.1002/pro.3509 (2019). [PubMed: 30239054]
22. Dore AS et al. Structure of class C GPCR metabotropic glutamate receptor 5 transmembrane domain. Nature 511, 557–562, doi:10.1038/nature13396 (2014). [PubMed: 25042998]
23. Frangaj A & Fan QR Structural biology of GABAB receptor. Neuropharmacology 136, 68–79, doi:10.1016/j.neuropharm.2017.10.011 (2018). [PubMed: 29031577]
24. Gasparini F & Spooren W Allosteric modulators for mGlu receptors. Curr Neuropharmacol 5, 187–194, doi:10.2174/157015907781695900 (2007). [PubMed: 19305801]
25. Pagano A et al. C-terminal interaction is essential for surface trafficking but not for heteromeric assembly of GABA(b) receptors. The Journal of neuroscience : the official journal of the Society for Neuroscience 21, 1189–1202, doi:10.1523/jneurosci.21-04-01189.2001 (2001). [PubMed: 11160389]
26. Balasubramanian S, Teissere JA, Raju DV & Hall RA Hetero-oligomerization between GABAA and GABAB receptors regulates GABAB receptor trafficking. The Journal of biological chemistry 279, 18840–18850, doi:10.1074/jbc.M313470200 (2004). [PubMed: 14966130]
27. Hyland NP & Cryan JF A Gut Feeling about GABA: Focus on GABA(B) Receptors. Front Pharmacol 1, 124, doi:10.3389/fphar.2010.00124 (2010). [PubMed: 21833169]
28. Ng TK & Yung KK Differential expression of GABA(B)R1 and GABA(B)R2 receptor immunoreactivity in neurochemically identified neurons of the rat neostriatum. The Journal of comparative neurology 433, 458–470, doi:10.1002/cne.1153 (2001). [PubMed: 11304711]
29. Burman KJ et al. GABAB receptor subunits, R1 and R2, in brainstem catecholamine and serotonin neurons. Brain Res 970, 35–46, doi:10.1016/s0006-8993(02)04269-5 (2003). [PubMed: 12706246]
30. Calver AR et al. The expression of GABA(B1) and GABA(B2) receptor subunits in the cNS differs from that in peripheral tissues. Neuroscience 100, 155–170, doi:10.1016/s0306-4522(00)00262-1 (2000). [PubMed: 10996466]
31. Gassmann M et al. Redistribution of GABAB(1) protein and atypical GABAB responses in GABAB(2)-deficient mice. The Journal of neuroscience : the official journal of the Society for Neuroscience 24, 6086–6097, doi:10.1523/JNEUROSCI.5635-03.2004 (2004). [PubMed: 15240800]
32. Margeta-Mitrovic M, Jan YN & Jan LY Ligand-induced signal transduction within heterodimeric GABA(B) receptor. Proc Natl Acad Sci U S A 98, 14643–14648, doi:10.1073/pnas.251554798 (2001). [PubMed: 11724957]
33. Xue L et al. Rearrangement of the transmembrane domain interfaces associated with the activation of a GPCR hetero-oligomer. Nature communications 10, 2765, doi:10.1038/s41467-019-10834-5 (2019).
34. Binet V et al. The heptahelical domain of GABA(B2) is activated directly by CGP7930, a positive allosteric modulator of the GABA(B) receptor. The Journal of biological chemistry 279, 29085–29091, doi:10.1074/jbc.M400930200 (2004). [PubMed: 15126507]

35. Galvez T et al. Allosteric interactions between GB1 and GB2 subunits are required for optimal GABA(B) receptor function. The EMBO journal 20, 2152–2159, doi:10.1093/emboj/20.9.2152 (2001). [PubMed: 11331581]
36. Guan XM, Kobilka TS & Kobilka BK Enhancement of membrane insertion and function in a type IIIb membrane protein following introduction of a cleavable signal peptide. The Journal of biological chemistry 267, 21995–21998 (1992). [PubMed: 1331042]
37. Mastronarde DN Automated electron microscope tomography using robust prediction of specimen movements. Journal of structural biology 152, 36–51, doi:10.1016/j.jsb.2005.07.007 (2005). [PubMed: 16182563]
38. Zheng SQ et al. MotionCor2: anisotropic correction of beam-induced motion for improved cryo-electron microscopy. Nature methods 14, 331–332, doi:10.1038/nmeth.4193 (2017). [PubMed: 28250466]
39. Zhang K Gctf: Real-time CTF determination and correction. Journal of structural biology 193, 1–12, doi:10.1016/j.jsb.2015.11.003 (2016). [PubMed: 26592709]
40. Rohou A & Grigorieff N CTFFIND4: Fast and accurate defocus estimation from electron micrographs. Journal of structural biology 192, 216–221, doi:10.1016/j.jsb.2015.08.008 (2015). [PubMed: 26278980]
41. Zivanov J et al. New tools for automated high-resolution cryo-EM structure determination in RELION-3. eLife 7, doi:10.7554/eLife.42166 (2018).
42. Pettersen EF et al. UCSF Chimera--a visualization system for exploratory research and analysis. J Comput Chem 25, 1605–1612, doi:10.1002/jcc.20084 (2004). [PubMed: 15264254]
43. Emsley P, Lohkamp B, Scott WG & Cowtan K Features and development of Coot. Acta crystallographica. Section D, Biological crystallography 66, 486–501, doi:10.1107/S0907444910007493 (2010). [PubMed: 20383002]
44. Liebschner D et al. Macromolecular structure determination using X-rays, neutrons and electrons: recent developments in Phenix. Acta crystallographica. Section D, Structural biology 75, 861–877, doi:10.1107/S2059798319011471 (2019). [PubMed: 31588918]
45. Lomize MA, Pogozheva ID, Joo H, Mosberg HI & Lomize AL OPM database and PPM web server: resources for positioning of proteins in membranes. Nucleic acids research 40, D370–376, doi:10.1093/nar/gkr703 (2012). [PubMed: 21890895]
46. Jo S, Kim T, Iyer VG & Im W CHARMM-GUI: a web-based graphical user interface for CHARMM. J Comput Chem 29, 1859–1865, doi:10.1002/jcc.20945 (2008). [PubMed: 18351591]
47. Humphrey W, Dalke A & Schulten K VMD: visual molecular dynamics. J Mol Graph 14, 33–38, 27–38, doi:10.1016/0263-7855(96)00018-5 (1996). [PubMed: 8744570]
48. Phillips JC et al. Scalable molecular dynamics with NAMD. J Comput Chem 26, 1781–1802, doi:10.1002/jcc.20289 (2005). [PubMed: 16222654]
49. Robertson MJ, Tirado-Rives J & Jorgensen WL Improved Peptide and Protein Torsional Energetics with the OPLSAA Force Field. J Chem Theory Comput 11, 3499–3509, doi:10.1021/acs.jctc.5b00356 (2015). [PubMed: 26190950]
50. Ryckaert J-P, Ciccotti G & Berendsen HJC Numerical integration of the cartesian equations of motion of a system with constraints: molecular dynamics of n-alkanes. Journal of Computational Physics 23, 327–341, doi:10.1016/0021-9991(77)90098-5 (1977).
51. Miyamoto S & Kollman PA Settle - an Analytical Version of the Shake and Rattle Algorithm for Rigid Water Models. Journal of Computational Chemistry 13, 952–962, doi:10.1002/jcc.540130805 (1992).
52. Laurent B et al. Epock: rapid analysis of protein pocket dynamics. Bioinformatics (Oxford, England) 31, 1478–1480, doi:10.1093/bioinformatics/btu822 (2015).
53. Ballesteros JA & Weinstein H in Methods in Neurosciences Vol. 25 (ed Sealfon Stuart C.) 366–428 (Academic Press, 1995).
54. Hilger D et al. Structural insights into ligand efficacy and activation of the glucagon receptor. bioRxiv, 660837, doi:10.1101/660837 (2019).
55. Towns J et al. XSEDE: Accelerating Scientific Discovery. Comput Sci Eng 16, 62–74, doi:Doi 10.1109/Mcse.2014.80 (2014).

56. Scheres SH Processing of Structurally Heterogeneous Cryo-EM Data in RELION. Methods in enzymology 579, 125–157, doi:10.1016/bs.mie.2016.04.012 (2016). [PubMed: 27572726]

57. Afonine PV et al. New tools for the analysis and validation of cryo-EM maps and atomic models. Acta crystallographica. Section D, Structural biology 74, 814–840, doi:10.1107/S2059798318009324 (2018). [PubMed: 30198894]

58. Kato K, Goto M & Fukuda H Regulation by divalent cations of 3H-baclofen binding to GABAB sites in rat cerebellar membranes. Life sciences 32, 879–887, doi:10.1016/0024-3205(83)90225-4 (1983). [PubMed: 6827916]

59. Bowery NG, Hill DR & Hudson AL Characteristics of GABAB receptor binding sites on rat whole brain synaptic membranes. 1983. Br J Pharmacol 120, 452–467; discussion 450–451, doi:10.1111/j.1476-5381.1997.tb06835.x (1997). [PubMed: 9142424]

60. Marheineke K, Grunewald S, Christie W & Reilander H Lipid composition of Spodoptera frugiperda (Sf9) and Trichoplusia ni (Tn) insect cells used for baculovirus infection. FEBS Lett 441, 49–52, doi:10.1016/s0014-5793(98)01523-3 (1998). [PubMed: 9877163]

61. Ma JC & Dougherty DA The Cationminus signpi Interaction. Chemical reviews 97, 1303–1324, doi:10.1021/cr9603744 (1997). [PubMed: 11851453]

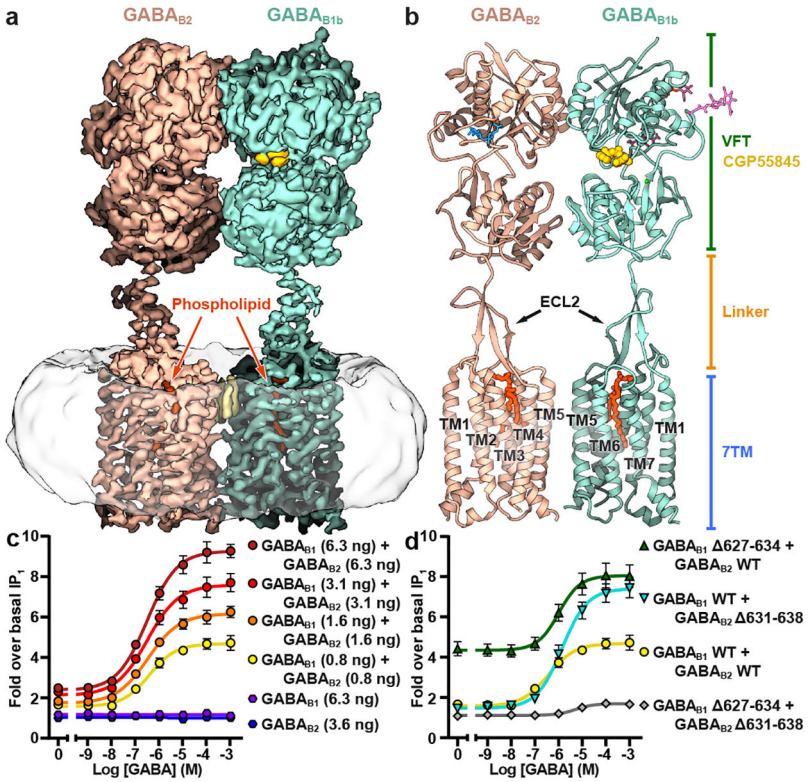

Figure 1. CryoEM map and model of the full-length GABA$_B$ receptor heterodimer in inactive state.

GABA$_B$ receptor cryoEM map (**a**) and ribbon diagram (**b**) (GABA$_{B1b}$: teal; GABA$_{B2}$:tan; GDN micelle: white; CGP55845: gold; phospholipids: orange; glycosylation: blue and pink). Elongated densities at the 7TM interface are likely lipid or detergent molecules (yellow). **c**, GABA E_{max} increases with higher levels of co-transfected GABA$_{B1}$ and GABA$_{B2}$ plasmid DNA. **d**, ECL2 truncation of either GABA$_B$ subunit increases E_{max} of GABA-stimulated response when compared to co-transfected wild-type receptors of similar surface expression (Extended Data Fig. 6a), but ECL2 shortening of both protomers inhibits activity.

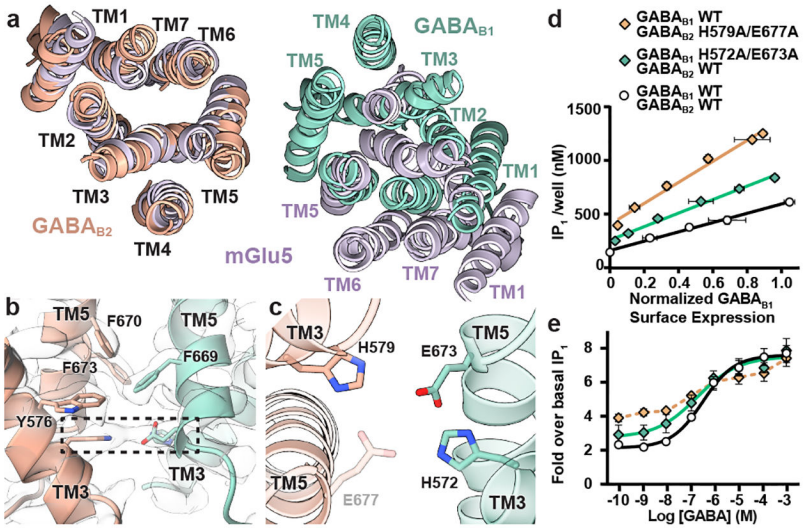

Figure 2. TM3 and TM5 stabilize an inactive-state dimer interface of GABA$_B$ 7TM domains.

a, Inactive-state GABA$_B$ 7TMs (GABA$_{B1}$: teal, GABA$_{B2}$: tan) are in closer proximity compared to those of inactive mGlu5 (purple; PDB:6N52), top-down view. **b**, The GABA$_{B1}$ and GABA$_{B2}$ interface is stabilized through hydrophobic interactions along TM5 helices and by polar residues on the intracellular side of TM3 and TM5 (boxed). **c**, Polar interaction residues from the intracellular side of the receptor. GABA$_{B2}$ E677 is shown for perspective; we note, however, that the map density for that residue was insufficient for high-confidence modeling of its side chain. IP$_1$ accumulation assays illustrate differences in GABA$_B$ TM3/5 mutants' basal activity, **d**, and GABA response, **e**.

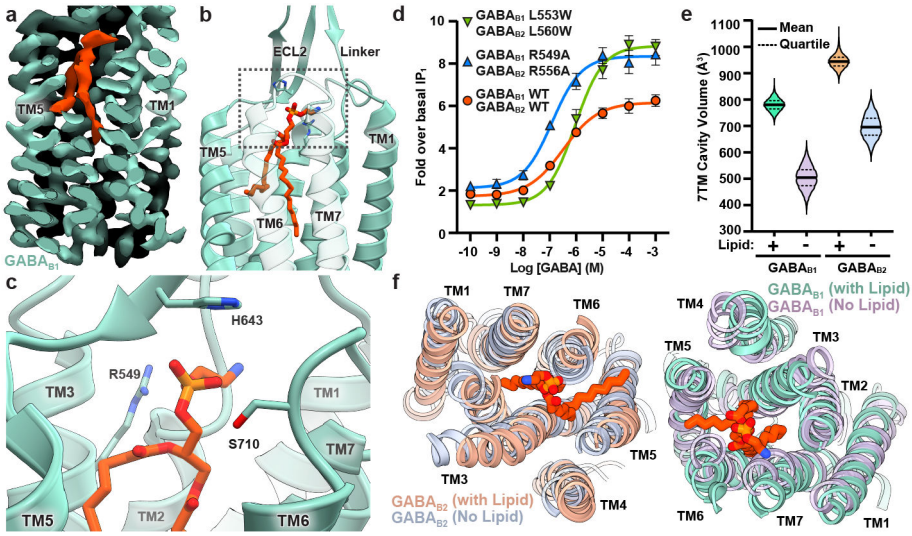

Figure 3. Phospholipid binds within the transmembrane cores of GABA$_B$.

a, EM map clipped to show the location of phospholipid within GABA$_{B1}$ of the heterodimer. Ribbon representation of PE within GABA$_{B1}$, **b**, with boxed region presented in panel **c** to show the structural environment of the headgroup. **d**, GABA concentration response for wild-type GABA$_B$ (red), and mutants designed to displace phospholipid (green), or de-stabilize the phospholipid headgroup (blue). **e**, **f**, MD simulations show a collapse of the transmembrane cavity when lipid is absent. **e**, Violin plot of cavity volume ensemble data. **f**, Representative top-down view of the GABA$_B$ ribbon and stick model from MD simulations at 200 ns.

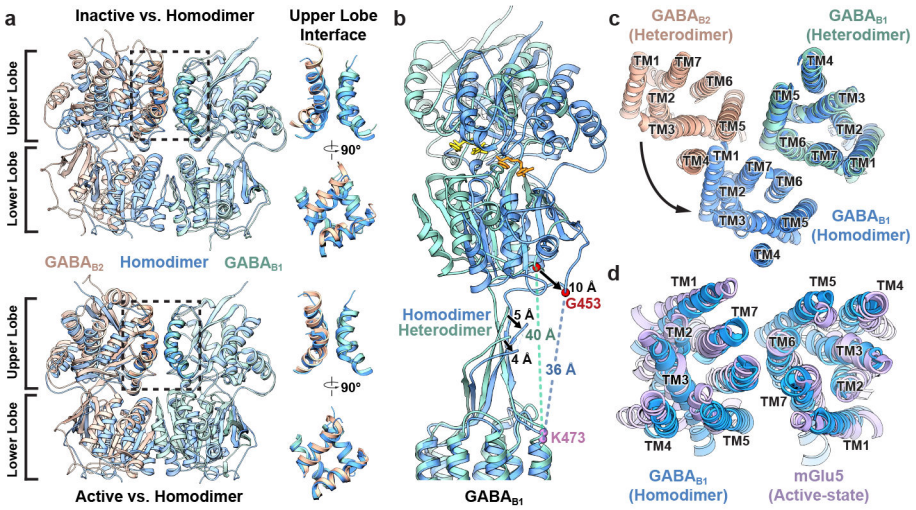

Figure 4. Inhibitor-bound GABA$_{B1}$ homodimers adopt similar VFT orientation as active GABA$_B$ heterodimer and similar 7TM interface as active mGlu5.

a, VFT overlay of crystal structures of GABA$_B$ heterodimer (tan, teal) in inactive-state (top) and active-state (PDB:4MS4)[12] (bottom) with the model of GABA$_{B1}$ homodimer (blue). The upper lobe interaction interface (boxed) of the GABA$_{B1}$ homodimer matches that of the active-state heterodimer. **b,** The GABA$_{B1}$ subunit of the heterodimer (teal) and homodimer (blue) were aligned to the 7TM domains, revealing differences in VFT and linker positioning. **c**, Top-down view of superposed 7TM domains of GABA$_B$ heterodimer (tan, teal) and homodimer (blue) showing the dramatic difference in protomer interface. **d**, Top-down view of superimposed 7TM domains of agonist-bound mGlu5 (purple, PDB:6N51[14]) and GABA$_{B1}$ homodimer (green).